BEYOND-DESIGN WIND ANALYSIS OF THE EUGENE TALMADGE MEMORIAL AND SIDNEY LANIER CABLE-STAYED BRIDGES

by

MAXIMILLIAN B. OVETT

(Under the Direction of Mi G. Chorzepa)

ABSTRACT

The objective of this thesis was to determine the response of cable-stayed bridges subjected to severe wind loading. A combination of static and dynamic wind loads were considered in order to be able to predict the response of Sidney Lanier and Eugene Talmadge Memorial cable-stayed bridges located on the coast of Georgia (USA). The bridges were assessed for beyond-design wind loading using the Saffir-Simpson hurricane wind scale. The method used mechanistically tested aerodynamic forces on bridge structures under high winds. Three-dimensional finite element models (FEM) were created to measure the internal force demand placed on the bridges by wind loading. The collapse of these two bridges would have significant economic impact on the state of Georgia. The analysis proved that the two bridges are vulnerable to Category 3 hurricanes and above. Both Sidney Lanier and Eugene Talmadge Memorial cable-stayed bridges should be closed in event of major hurricanes.

Index Words: Cable-Stayed Bridge, FEA (Finite Element Analysis), Beyond Design, Wind, Dynamic, Hurricane

BEYOND DESIGN WIND ANALYSIS OF THE EUGENE TALMADGE MEMORIAL AND SIDNEY LANIER CABLE-STAYED BRIDGES

by

MAXIMILLIAN B. OVETT

B.S., The University of Georgia, 2016

A Thesis Submitted to the Graduate Faculty of The University of Georgia in Partial Fulfillment of the Requirements for the Degree

MASTER OF SCIENCE

Athens, Georgia

2017

BEYOND DESIGN WIND ANALYSIS OF THE EUGENE TALMADGE MEMORIAL AND SIDNEY LANIER CABLE-STAYED BRIDGES

by

MAXIMILLIAN B. OVETT

Major Professor: Mi G. Chorzepa

Committee: Stephan A. Durham

Jason Christian

R. Benjamin Davis

Electronic Version Approved:

Suzanne Barbour

Dean of the Graduate School

The University of Georgia

December 2017

DEDICATION

My thesis is dedicated to everyone who has generously taken time out of their lives to provide me with their guidance and education. I am especially grateful to my teachers, counselors, and stewards at the Northwood Elementary School in Roswell, Ga. Without them I would never have reached where I am today!

ACKNOWLEDGEMENTS

I want to offer my sincere appreciation to everyone who has helped me in reaching this point. Thank you, to Dr. Mi Geum Chorzepa for being my mentor and providing me with the opportunity to work with her on such a challenging topic. Thank you, to my committee members Stephan Durham, Jason Christian, and Ben Davis who have given feedback and guidance. Lastly, I want to thank my father and mother for instilling me with ability to honor my commitments, to always ask questions no matter the size or spectrum, and supporting me in all my endeavors.

TABLE OF CONTENTS

LIST OF TABLES

LIST OF FIGURES

1. INTRODUCTION

1.1 Background

Cable-Stayed Bridges are becoming ever more prevalent in today's society; they fulfill numerous different needs. Primarily these bridges connect two distant locations in a cost effective manner. They also are a focal point and an emblem for the community. Yet for all of the positive benefits of cable-stayed bridges, the knowledge of loading scenarios and failure mechanisms is limited. A study of the performance of cable-stayed bridges through the development of in-depth analytical models was undertaken in order to gain a better understanding of the performance of cable-stayed bridges.

Cable-stayed bridge structures present a number of different aerodynamic challenges. Due to reduced weight, high flexibility, and low damping coefficients, cable- supported bridges are vulnerable to environmental events such as hurricanes and tropical storms. Experimental wind tunnel testing on scaled models is performed during the development stages of cable-stayed bridge designs. The wind tunnel testing generally places a scaled section of the bridge into the path of a statistically determined wind speed to evaluate the global deflected shape, natural frequencies of vibration, and flutter on set speeds. Furthermore, adjustment of the winds angle of incidence (the angle on which the wind first touches the bridge deck) to the bridge is investigated in order to determine the largest global deflection. .

The field of structural health monitoring is growing and has the potential to provide valuable information about the condition of bridges over time. Sensors are incorporated into bridge structures in order to assess the overall strain on and maximum deflection developed within

bridges during large storms. Through monitoring and collection of data from these sensors on existing cable-stayed bridges, it is possible to provide information on the performance of different cable-stay configurations in complex and dynamically changing environmental conditions. Such health monitoring allows analysis of the force paths and determination of areas with high stress and locations of likely failure.

Analytical modeling provides engineers with an array of tools and approaches to measure the behavior of cable-stayed bridges and determine the natural frequencies of the structures. These frequencies are used as the basis for further analysis. Fluid modeling, either computational or experimental, provides visualization of the vortices created by the fluid structure interaction.

Wind effects on cable-stayed bridges are modeled by means of the modal superposition method [RWDI 1996] or by using a statistical approach based on a frequency response function (FRF) leading to power spectral density (PSD) graphs. These approaches evaluate a mean static force; they also take a modal superposition of the dynamic response from either the mode shapes in the former method or the resonant responses identified in the FRF and PSD graphs in the latter method. The static and dynamic responses inform the engineer of the probable wind loading on the cable-stayed bridge structure.

Due to the availability of powerful computing hardware, it is possible to generate full three dimensional models of cable-stayed bridges structures. These models allow engineers to run multiple dynamic analyses at faster rates than ever before and provide more insight and understanding of the bridge's response. It is now even possible to incorporate a decade's worth of recorded weather data as input to three dimensional CFD models, enabling users to understand how new or current cable-stayed bridges withstood past storms and provide insight into how they

will withstand present and future storms. This type of research is invaluable since it provides engineers with greater understanding of bridges for beyond-design basis loading.

1.2 Literature Review

1.2.1 Review of Cable-Stayed Bridge Analysis Procedures

The first part of this study focuses on understanding the underlying structural dynamics of cable-stayed bridges and their supporting structures. This was primarily accomplished through a review of published literature on the subjects of bridges, wind, and vibration analyses. Overall, little was found on the on the subject of failure analysis of long-span bridges, specifically due to wind forces. There are several articles about equivalent static wind loads on cable-stayed bridges. However, the articles which focus on static force functions do not provide much detail on the dynamic response (Yang 2012). These static forces are associated with providing a drag force, lift force, and pitching moment determination on the bridge deck section. The literature does little to explain how best to represent dynamic forces and moments on the bridge.

1.2.2 *Representation of Dynamic Response*

Several different perspectives are available in literature on how to represent the dynamic response of a cable-stayed bridge. Yang et al. (2012) used a statistical approach to determine background forces seen on the bridge, resulting in loads resembling sine and cosine functions (Yang 2012). A recent study is beginning to highlight the dynamic contributions through an "evolutionary random process with time varying mean" (Chen 2015). This process involves an iterative method based on stepping through loading and reloading scenarios of the static deflected shape. Further evaluation of this statistical method counting for mean, resonant, and background forces for loading has been experimentally studied within wind tunnel tests (Iriwin 1995).

Another approach assess gust loading as a dynamic portion for the total load (Davenport 1967). This method proves useful but requires a full wind tunnel test to actually incorporate the structure's behavior at low and high wind speeds. Expanding upon the equations used for gust loading, Holmes et al. (Holmes 2002) uses the same approach but rearranges the formulation of the equations to better represent a long span bridge's behavior. Common practice in analytically combining multiple dynamic terms is to use square root of sum of squares, SQRSS (Jones 1998). An alternative approach, rather than using SQRSS, is to use a complete quadratic combination, CQC method. This method shows agreement with the SQRSS method but has the advantage of the dynamic response being directly calculated (Fu 2008).

1.2.3 *Flutter, VIV, and Local Vibration Problems*

The aerodynamic wind forces result in vibrations of the bridge-deck and cables which can cause torsional divergence, flutter, galloping, and ultimately collapse (Elsa de Sa Caetano 2007; Yang 2012; Larsen 2015; Frýba 2001; Nielson 2005). Even for aerodynamically stable girder sections which have been optimized to obtain better flutter performance, another kind of self-excited vibration such as vortex-induced vibration may occur at lower wind speed range (Irwin 1995). While galloping is not commonly encountered in cable-supported bridges, vortex shedding is a highly anticipated phenomenon. To suppress vortex induced oscillations of the bridge girder, a guide vane is sometimes added below the deck section (Davenport 1984). Furthermore, rain-wind induced cable vibrations have been reported for a relatively low wind velocity. The vibration appears to cease at a wind velocity of around 14 m/s (Chorzepa et al. 2016).

1.2.4 *Wind Tunnel Test vs. CFD Analysis*

Within the literature, there is little a focus on how to predict the global response of a long-span bridge subjected to wind loads. In addition to the dynamic response (buckling and flutter), previous studies described how the shapes of the bridge deck affect overall behavior under various loading conditions. A case study by Raggett et. al. (2016) looked into different modifications to the decks of cable-supported bridges; they described how sometimes minor changes in behavior changed the global structural response. These tests were all performed within a live wind tunnel and demonstrated the importance of deck geometry in determining the wind speeds a bridge can handle. In the case of the Lion's Gate reconstruction, the existing bridge had to be brought up to allowable construction standards to begin work (Raggett 2016); this was done by the addition of covers on the walkway. As a result, these covers became aerodynamic dampers that increased the wind speed at which flutter occurred.

A numerical method using Theodorsen functions has been shown to yield accurate results using a linear aero elastic set of equations that determines motion induced forces (Sukamta 2017). This study used a three-dimensional computational fluid dynamics model (Kim 2014) and compared the results with a two-dimensional model. Their analysis highlighted the importance of performing a dynamic analysis. The authors conducted both a modal analysis to determine frequency and displaced shapes versus a full CFD analysis using an iterative solver method. These results demonstrated how the contributing modes and deformed shapes were similar to that of the CFD results. This study's findings inform researchers on the type of analysis that needs to be performed depending on the result and time required, particularly in the absence of the wind tunnel test results.

1.2.5 *Identification of Failure Mechanism and Vulnerable Elements*

It is important to understand the wind forces and the different evaluation approaches used to predict the global response of long-span bridges. It is equally important to know the failure mechanisms and collapse patterns for long span bridges, particularly cable-stayed bridges. The identification of critical components and their overall influence on a structure is paramount. If failure of a cable occurs, it is important to identify which cable(s), could lead to the collapse of the entire structure, be it progressive or immediate. Dos et al. (2016) found that failure of the outer cables, are more likely to lead to overall collapse of the bridge due to the large amount of forces released and redistributed during failure.

1.2.6 *Modeling Methodology and State-of-the-Art Methods*

In finite element analysis (FEA) modeling procedures, it is typical to represent the cable elements by a link element. The link element model factors only tension, which results in an iterative nonlinear analysis and highlights cable dynamics. An approach using a beam element as the connecting element between cables and towers or deck appears to be a promising compromise (Xuewei 2017). The beam element model yields or fails when the axial forces reach a certain limit. Further applications of recorded wind or seismic events are used to input for loading (Xuewei 2017). By understanding the correlation between analytical models and loading input, it is possible to equip long span bridges with accelerometers and geo-spatial recording devices and GPS, to record the dynamic behavior of bridges that are exposed to large trauma events. Han et al. (2016) proposes a three-tier system of recording devices including GPS receivers, accelerometers, and anemometers. Using the above collected data inside an analytical model has led to a reduction of deck stiffness around 14 to 16% (Huynh 2016). This type of reduction has a large effect on the distribution of forces within the overall structure.

1.3 Problem Statement

Understanding the response of a cable-stayed bridge to wind forces, in particular those of a large magnitude, is important in order to determine how likely failures are to occur due to beyond design-basis wind forces. and how they influence the global response of long-span bridges. Cable-stayed bridges are readily open to wind excitation forces, leaving them vulnerable to major hurricanes. These aerodynamic forces result in vibrations emanating throughout the bridge-deck, cables, and supporting towers. Vibrations can cause torsional divergence, flutter, galloping, and ultimately self-destruction (Ataei 2013, Padgett 2008, Schemmann 1998, Wu 2012, Li 2013).

While cable stayed bridges are widespread in Asia and Europe, they are just now increasing in number in North America; they are primarily located on the Mississippi River, Ohio River, and the Eastern Seaboard (Chorzepa et al. 2016). Cable-supported, precast/post-tensioned concrete bridges are generally flexible structures that are easily excited by wind loading. The excitation forces acting on cables and cable-supported concrete bridge superstructures are aerodynamic by nature. However, the result of these forces is highly dependent upon the underlying structural dynamics of the bridge structures. For a concrete bridge girder, aero-elastic instability may develop as torsional divergence or flutter. Torsional divergence occurs when the total aero-elastic stiffness becomes negative, and any small perturbation of the concrete girder's at-rest state can become magnified and result in a sudden failure (Caetano 2007, Yang 2012). Flutter, on the other hand, is due to negative aerodynamic damping and is characterized by a rapid build-up of intense torsional and vertical vibrations potentially leading to collapse (Yang 2012).

This research studied the Sydney Lanier cable-stayed bridge in Brunswick, Georgia and the Eugene Talmadge Memorial cable-stayed bridge in Savannah, Georgia. These bridges, being near the coast,

are subjected to high wind loading and are in the direct path of hurricanes. These bridges have been in service since 2003 and 1993, respectively, with an estimated cost of ~$65 million to construct. Both bridges have been closed to traffic several times due to the imminent threat of major hurricanes such as Matthew and Irma, without much understanding of their underlying behavior.

1.4 Objectives and Scope of Study

The goal of this study was to develop a method to be able to analytically predict and understand the dynamic response of cable-stayed bridges during beyond design-basis windstorm events or major hurricanes.. Previous studies concerning wind analysis of cable-stayed bridges mainly focused on the local vibration problems such as flutter, Vortex-Induced Vibration (VIV), and/or cable vibrations. In contrast, few studies have investigated the influence of escalated wind forces on the global failure response of cable-stayed bridges. This study included a wind analysis of the Sidney Lanier and Eugene Talmadge cable-stayed bridges. The research focuses on understanding the underlying structural dynamics of cable-stayed bridges and their supporting structures.

The ultimate goal of this study is to be able to predict the global response of the cable-stay bridges in order to provide criteria for the Georgia Department of Transportation to use in making a decision as to whether the bridge should remain open to traffic during beyond-design basis wind events. Furthermore, this study will provide a better understanding of estimated financial losses associated with future hurricane events.

This goal will be achieved by developing a finite element analysis model and studying dynamic mode shapes of both the cable-stayed bridges in Georgia. The Eugene Talmadge Memorial and Sidney Lanier Bridges models are constructed in a finite element analysis program

to determine the vibration modes of the bridge. The evaluation of dynamic performance and global response in peak winds and large-scale hurricanes is presented herein. The primary intent of this research is to determine if and when the Sidney Lanier and Eugene Talmadge cable-stayed bridges fail due to wind and not to predict the progressive nature of failure through a redistribution of forces utilizing nonlinear concrete and reinforcing steel material models, although geometric nonlinearity from the large deflection is considered. This study is intended to provide a simplified method practical for conducting a linear elastic wind analysis and interpreting the results used a concrete section analysis. The Eugene Talmadge Memorial and Sidney Lanier Cable-Stayed bridges shown in Figs. 1 and 2, respectively, are post-tensioned reinforced concrete structures.

Figure 1 **- The Eugene Talmadge Memorial Cable-Stayed Bridge [20]**

Figure 2 - The Sidney Lanier Cable-Stayed Bridge [21].

1.5 Summary of Chapters

The thesis consists of six chapters. Chapter One introduces the topic of cable-stayed bridges and provides the reader with necessary background information on the importance cable-stayed bridges. It also, highlights different areas of research that are being pursued. Chapter One finishes by defining the problem statement and overall scope of the research. The Chapter Two describes how the finite element model (FEM) was developed. This chapter thoroughly describes how interpretation of the construction documents, drawing of the overall geometry, and meshing of the entire structure was completed. The Chapter Three covers the validation and verification of the FEM model, a step critical in insuring that the model produces accurate and valid results. The Chapter Four discusses the analysis method and procedures of how the beyond-design wind application is completed for both of the two bridges under investigation. The fourth chapter continues the interpretation of the results for each individual bridge as well as a comparison between the two bridges. Chapter Five discusses the overall results and provides suggestions for where and how this work could be used in future research and in the field of civil and bridge engineering. Chapter Six consists of the overall conclusions and provides recommendations for how these results should be used for both public and state agencies.

2. DESCRIPTION OF THE FEA MODEL

2.1 Introduction to Modeling and Modifications

This project digitized the geometry of both the Eugene Talmadge Memorial and Sidney Lanier cable-stayed bridges. The Sidney Lanier bridge was digitized first due to better overall documentation as shown in Fig. 3. Digitizing the Sidney Lanier bridge first provided a large amount of learning experience in performing three dimensional geometry generation which was then implemented in the digitization of the Eugene Talmadge Memorial bridge shown in Fig. 4. Both bridges were conceptualized from construction documentation provided by GDOT. This documentation provided all lengths, widths, and thickness of all components, as well as necessary elevation stations to ensure that the geometry was created accurately.

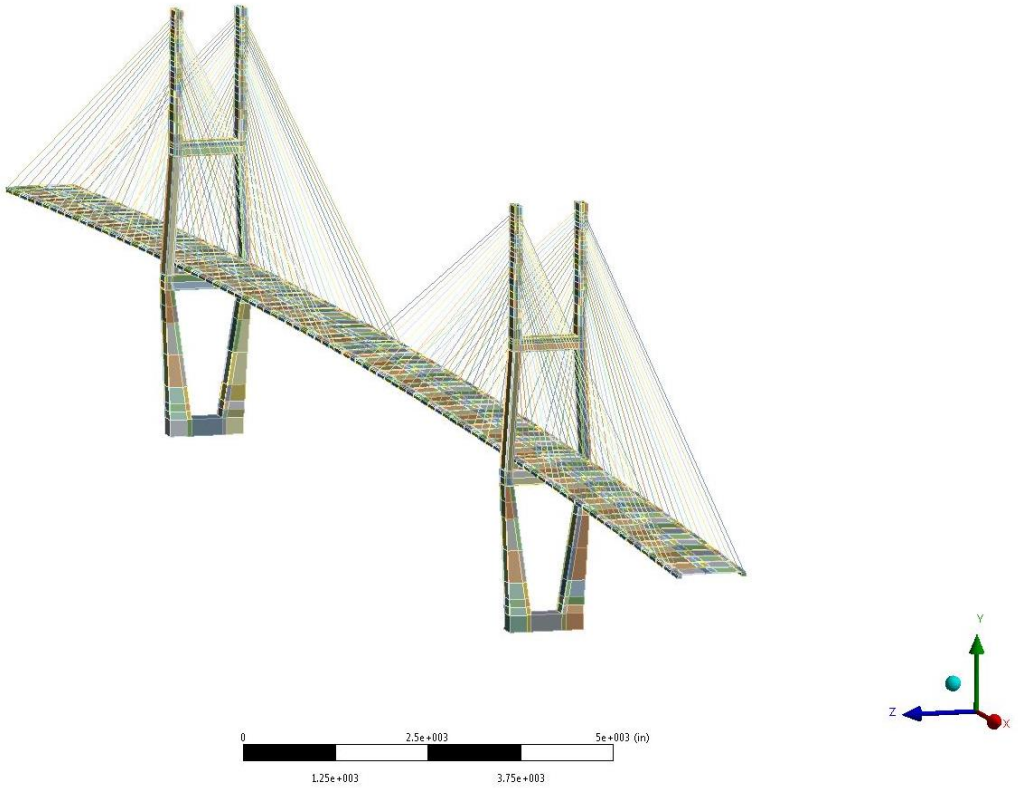

Figure 3 - Isometric View of Sidney Lanier Cable-Stayed Bridge.

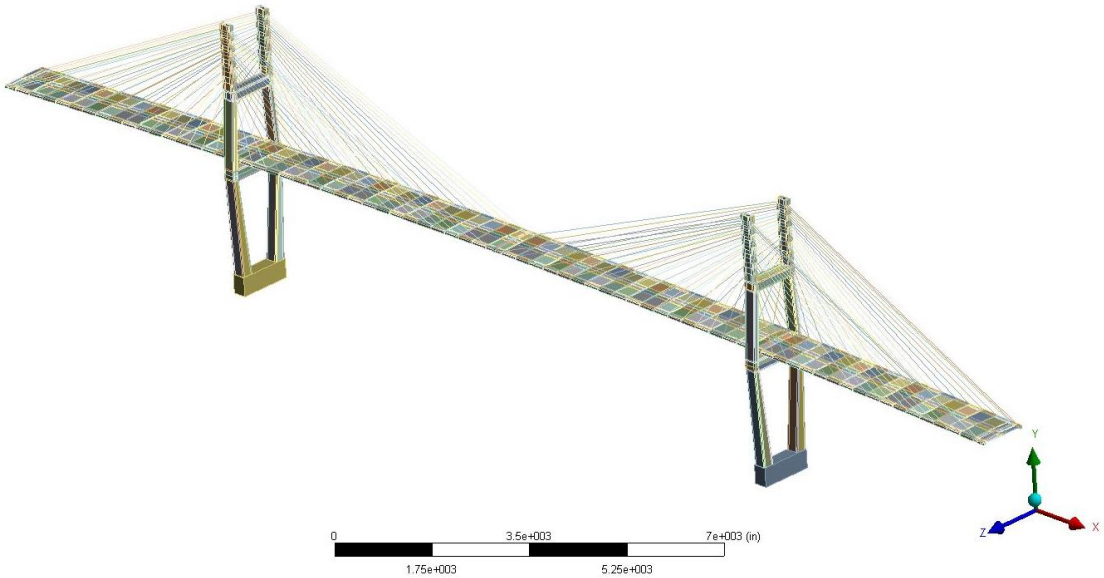

Figure 4 - Isometric View of Eugene Talmadge Memorial Cable-Stayed Bridge

The model was separated into three components: the bridge deck, the bridge towers, and the cables. The separation into these components was important for a two reasons: (1) it reduced the overall load placed on the available computational resources (2) it allowed the user to better perform quality control on the model since each component could then be individually analyzed and verified for appropriate behavior.

The selection of computer aided graphic design (CAD) packages is entirely up to the person drawing the geometry, as long as the necessary geometry required for modeling can be imported to ANSYS mechanical. Two different CAD packages were used for this project: Design Modeler and SpaceClaim. Both are provided by the ANSYS Workbench software.

There were a few augmentations made to bridge geometry. First, the two cross-ties within the towers were extruded to the thickness of 6.71 m (22ft), which is the same thickness of the towers. The construction documents call for the two cross-ties in either bridge to be inset by 1ft on either side of the tower. Thus, a total thickness of 6.71 m (22 ft) is used rather than 6.10 m (20ft). This change in geometry was made to provide a superior mesh between the two different components of the tower. The elastic modulus is slightly adjusted to accommodate this change.

The transverse beams underneath the deck have been moved slightly forward such that the beam lies directly beneath the cable. This change was made so that the force of the cable directly translated into the beam is more realistic. In actuality, the cables pass through the bridge deck and into steel stiffeners which are within the transverse beam, providing the anchorage for cables. Furthermore, the chamfering of the transverse beam to either side of the deck has been removed for each beam in order to simplify geometry and achieve mesh compatibility between different components.

2.2 Creating the Geometry

The towers in the models are symmetric, and thus only one tower for each model needed to be created for mirroring. An efficient approach to drawing these towers was to create a surface in the X-Y plane then extrude that surface in the Z direction creating the full 3-dimensional drawing. This method was optimal because it allowed specific points of the tower to be keyed in the lines and surfaces created between those points. The points chosen were lower tower legs, 1st cross-tie, mid tower legs, 2nd cross-tie, and upper tower legs. Once all of the points were in and the surfaces created, they were extruded to the appropriate thickness and planes were created at the correct location to divide the geometry appropriately. This allowed the use of the subtraction 'Boolean' operation to remove the center core of the towers and cross-ties thus rendering a hollow core structure. Creating the discrete point to attach the cables was done by slicing the geometry at the coinciding elevation where the cables entered the tower, as well as at the center line of the top legs in the longitudinal direction of the deck. Creating a vertex at the point of contact between the tower and cables allowed for easier attachment of cables in future stages (i.e., meshing operation).

The deck has an overall grade from apex to end of 5.5%, shown in Figs. 5 and 6. Given that the shape was not a linear straight line but was instead a large sweeping parabola, the spline tool was used to draw the path of the deck in the longitudinal direction.

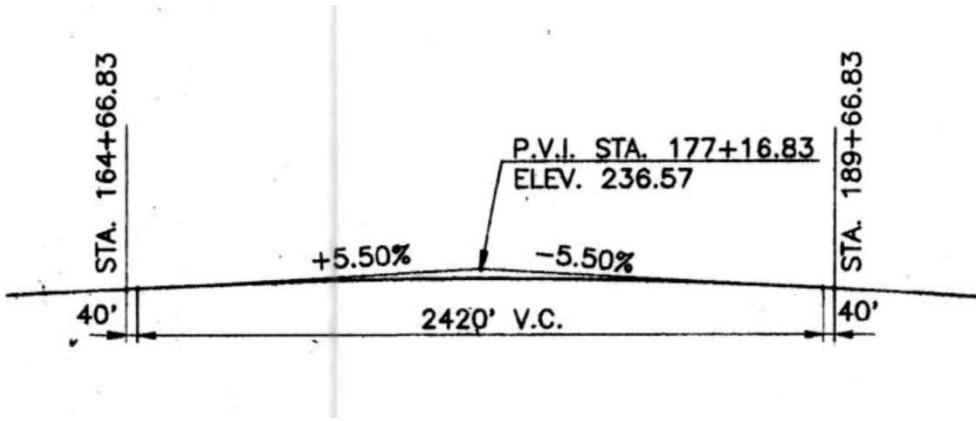

Figure 5 - GDOT Construction Documents Specified Grade

Three discreet points were used to define the longitudinal profile shown in Fig. 6, and a polynomial of the second order was created when using the spline tool, creating a desired parabolic profile.

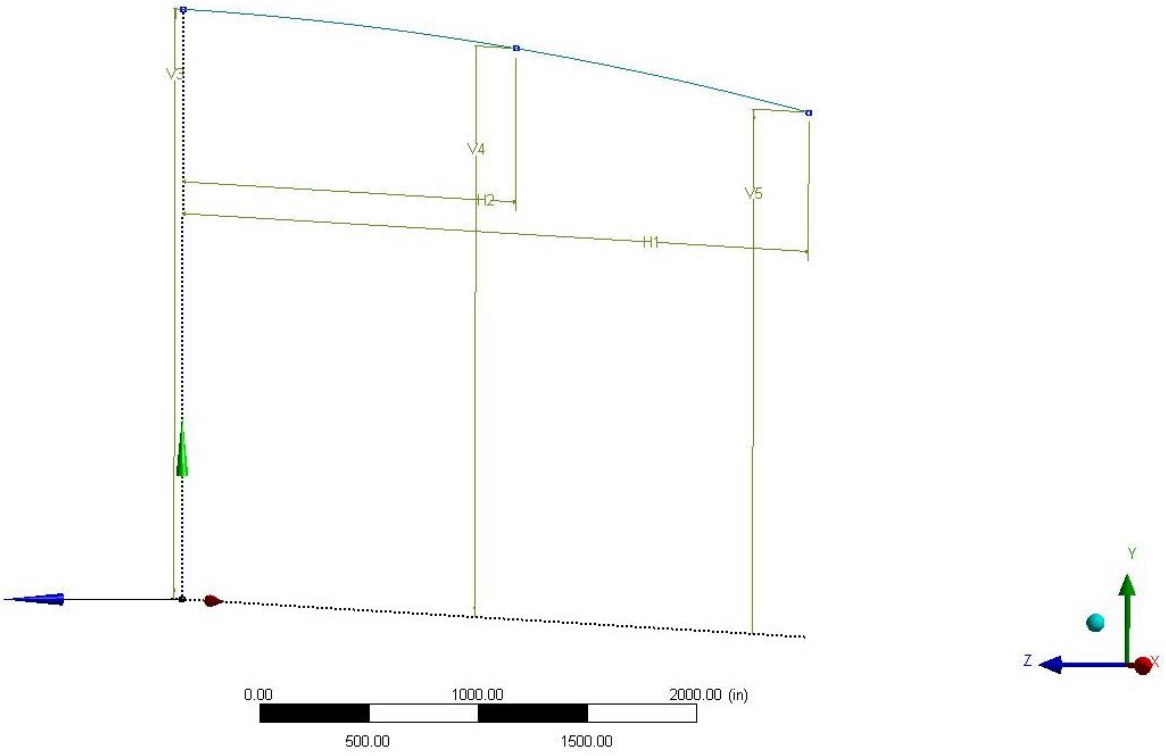

Figure 6 - Half-Span of Bridge Created With Spline Tool Using 3 points

The cross-section of the bridge decks were separated into 16 different surface areas shown in Fig. 7 and then extruded along the defined spline to create a three dimensional solid body. Two separate distinctions needed to be made about the deck. A portion of the deck is hollow, and another portion of the deck which is coincident with the transverse beam.

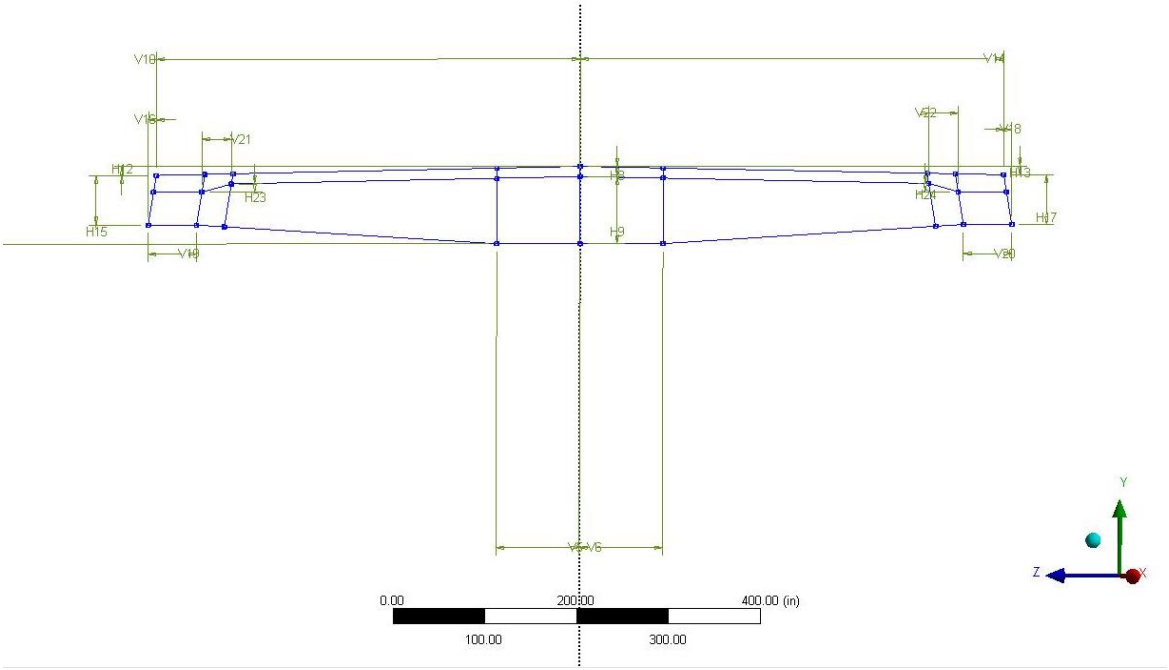

Figure 7 - Surface Profile Drawn for the Deck and Transverse Beam

Having extruded multiple solid body sections along the defined path of the deck planes, plane section divisions in the longitudinal direction were placed at specific intervals along the length of the deck, as defined by the locations of the transverse beams. By placing the planes at the correct location along the deck and then slicing normal to the deck at the exact location, the transverse beams were created. Having defined the transverse beam bodies, a 'Boolean' operation of subtraction was used within the ANSYS program to subtract out unnecessary volumes.

To ensure that the cable ends are coinciding with the correct locations for both the tower and deck, construction points were used. The coordinates for these construction points were

found within the construction documents allowing for an excel file to be created that held the X, Y, and Z locations for each point shown in Fig. 8. After importing these points into the CAD program, the command of creating lines from points was implemented generating the necessary line bodies used to represent the cables.

	A	B	C	D	E
1	#Group	Point	X_Cord	Y-Cord	Z-Cord
2	1	1	-476.165	206.129	38.25
3	1	2	-468.166	206.52	38.25
4	1	3	-460.166	206.908	38.25
5	1	4	-432.03	208.249	38.25

Figure 8 - Example of Created Coordinate File Used to Create Cable Geometry.

2.3 Development of the FEA Model

The 3D models of the Eugene Talmadge Memorial and Sidney Lanier cable-stayed bridges were created utilizing CAD packages. Inside each model, the bridge was sub-divided into multiple components: the towers, deck, and cables. This sub-division was to enhance computational efficiency and sub-modeling conformation of each bridge component. All aspects of the tower are of linear geometry, and the bridge deck has a non-linear parabolic geometry.

The creation of a solid 3D model is one of the more difficult models to create. The other option for this model would have been to use beam-shell geometry to represent the two different cable-stayed structures. A beam-shell model would have been easier to draw in that lines and surfaces would represent the structure. However, after assessing the objective of this project, it was determined that a beam-shell model would have been insufficient. It has been discussed above that the model was separated into multiple sub-components. These two bridges models could have been created without sub-components. This would have yielded less issues with

connections between components, meshing operations, and overall time it takes to update the model. This was decided against due to the amount of computational resources currently available. Furthermore, sub-components allowed for easier change and conformation of geometry. The cable cross-sectional profile was defined as an equivalent amount of steel area. This choice was made based on the objectives of the project being interested in overall global behavior of the bridge and not localized behavior of the cables.

2.3.1 Meshing of the Bridge Geometry

Meshing is the process which formulates mathematical equations to represent the cable-stayed bridge structure. This includes all three components of the bridge: being the cables, bridge deck, and towers. The meshing for this project was performed within ANSYS 16.2 Mechanical platform. This platform allows the user to import drawn CAD geometry and then create elements and nodes within this geometry. During the meshing procedure, the user must determine the optimal mesh quality for convergence of solutions. The more refined the mesh is, the more accurate the results of the analysis are because the solutions converge.

However, refined mesh requires larger computational capacity. Within ANSYS 16.2 Mechanical, it is possible to let the program decide the meshing procedure. The quality of mesh generated by this auto-meshing feature is highly dependent on the complexity of the geometry and for cable-stayed bridges, geometry yielded poor results. Furthermore, it was desired to mesh the cable-stayed structure with cubic elements as much as possible due to the fact that cubic elements yield more accurate results and are computationally more efficient than tetrahedron elements. To achieve this desired mesh quality, the user must constrain the geometry through a number of different manners such that when the meshing operation is performed, the desired mesh will be

produced. The constraints were applied by selectively 'slicing' the bridge components in specific manners as well as applying specific requirements for the size of the required elements.

2.3.2 Theory

A finite element model consists of selecting a mathematical equation that can be used to represent the behavior of interest. The mathematical equation of interest is then placed into a weak form notation. Then, an approximate and trial solution must be defined along with an appropriate weight function. After these steps, the weak form needs to be expressed in the form of matrices and vectors and then evaluate the element stiffness matrix and element body force vector for all elements**.** Subsequently, assembling the element matrices and vectors to produce the global governing equation with the application of boundary conditions to reduce governing equations and by solving the reduced weak form of the equations for the solution. This creates a 3-dimensinal discretization of the entire bridge structure. This divides the structure into many small elements with each element being composed of a specific number of nodes. Each of these elements can be described by how it moves and rotates in the X, Y, and Z direction. Each of these elements has specific properties such as mass and stiffness. Thus, they can be combined to form a large (or global) stiffness matrix that mathematically represents the overall structure. The mathematical stiffness formulation and solution algorithm of the bridge model is handled within ANSYS 16.2 Mechanical. The cable-stayed bridge is meshed using multiple different element types found in Table 1.

Table 1 - Elements Used in Cable-Stay Bridge

Structure	Element Type
Bridge Deck	solid186
Tower	solid185
Cables	beam188, link10

2.3.3 Mesh Convergence

The goal during meshing is for the object being meshed to reach convergence. Convergence is when the solution is nearing the theoretical exact solution or the error in displacement/strain solutions is minimized. The mesh has been refined to reach convergence when the solution being produced no longer changes with an increase in the number of elements as shown in Fig. 9.

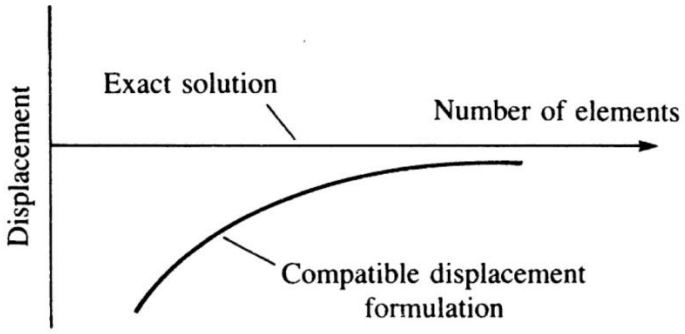

Figure 9 - Convergence and Mesh Refinement.

To ensure that the cables, deck, and towers for the cable-stayed bridges are meshed appropriately, multiple different mesh sizes were studied. To ensure that convergence of the bridge deck had been achieved, and to ensure that the computational time required to solve the model was minimized, each component was studied individually before being brought together within the

whole model. This enabled the evaluation of effects of mesh size and quality on the overall convergence to be studied. The whole model is also studied for convergence.

2.3.4 Towers

The tower was meshed using cubic or 'solid185' elements made up of 8 nodes as shown in Fig. 10. Each node has three degrees of freedom. Appropriate 'slicing' of the geometry is needed to allow for the best mesh to be achieved. The tower was sliced be made up of only squares, rectangles, and trapezoids. Two way slicing of the tower legs and crossties was completed such that separate corner bodies were created. This allowed for a higher quality mesh throughout the tower structure. Bodies between the tower legs and cross-ties were further sliced to create separate volumes. The towers fully meshed are presented in Figs. 11 and 12.

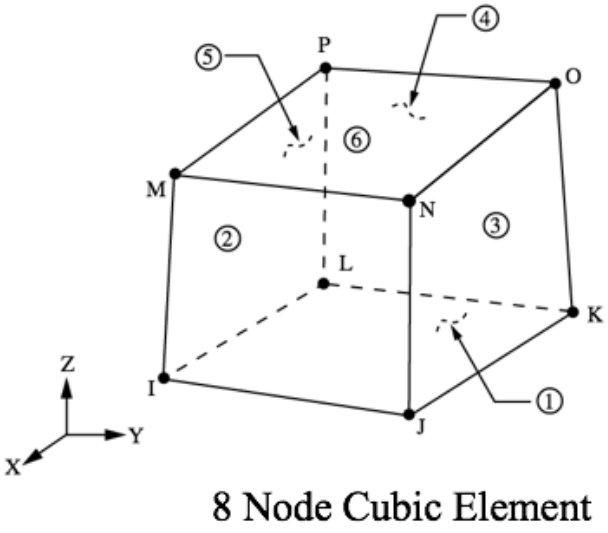

Figure 10 - Solid 185 element (SAS IP 2016).

Figure 11 - Sidney Lanier Meshed Towers.

Figure 12 - Eugene Talmadge Memorial Meshed Towers.

2.3.5 Deck

The meshing of the deck with a hex dominant meshing operation proved to be a challenging task. This was due to the curvature of the deck. To overcome this challenge and keep a computationally efficient mesh, the ‘solid 186’ element was used. Solid 186 is an element of cubic nature and is made up of 20 nodes as shown in Fig. 13. Each node has three degrees of freedom. This increases in number of nodes from 8 to 20 and allows for a better representation of the deformation due to the ability of the element to have slightly skewed angles between nodes. Slicing operations were performed on the deck volumes to ensure that a refined mesh was produced at cable anchorage locations. The deck was sliced in such a way to create 18 separate bodies within a component. This was done such that hex elements are generated for assignment of ‘solid 186’. Edge constraints were also applied to both the vertical and transverse directions of the bridge deck, enabling the optimal number of elements to be created within the mesh.

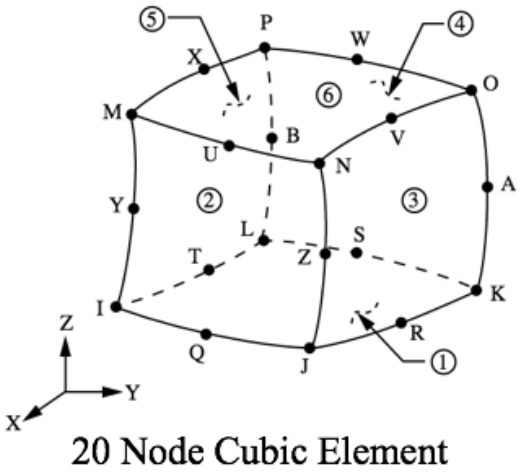

Figure 13 - Element Used to Mesh the Deck (SAS IP 2016).

2.3.6 Cables

The cable component for these cable-stayed bridges posed a large challenge due to the desired behavior of the component. In theory, cables are designed to work only in tension and cannot translate any rotational forces in X, Y, and Z directions to the attached bodies (i.e., the bridge deck and tower). Two different elements have been selected to represent the cable behavior, which are 'beam188' and 'link10' shown in Figs. 14 and 15. 'Beam188' cable elements were used for a modal analysis whereas 'link10' elements were used within the static analysis. The 'beam188' element is a cubic 2 node beam element where each node has 6 degrees of freedom. The 'link10' is a three-dimensional spar element that can be programmed to allow for tension only, and each node has only three-degrees of freedom translation in the X, Y, and Z directions.

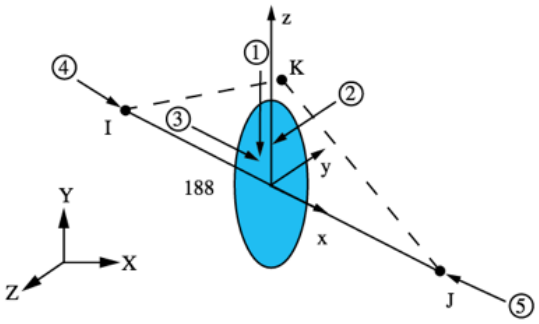

Figure 14 - Beam188 Element (SAS IP 2016)

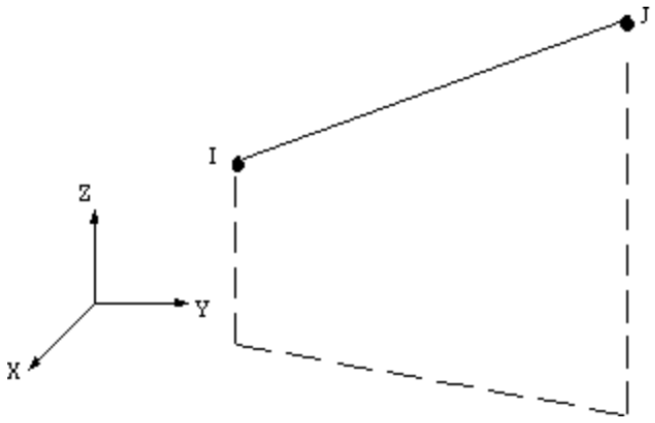

Figure 15 - Link10 Spar Element (SAS IP 2016).

2.3.7 Discussion

The choice of elements within the two cable-stayed bridges was based on their computational efficiency as well as their ability to accurately represent the structures in question. It is possible to use other element types and allow the ANSYS program to generate an automatic mesh. While this option is useful for a basic analysis, it can lead convergence problems. Two types of elements are used for the cables due to the ANSYS Workbench software's limitations. The 'link10' element is the most appropriate element to be used within the software. However, this element is not used in dynamic analysis, because this element type is not available for a modal analysis, and thus leaving 'beam188' as the best element choice. The overall meshed structure of each bridge is illustrated in Figs 16 and 17.

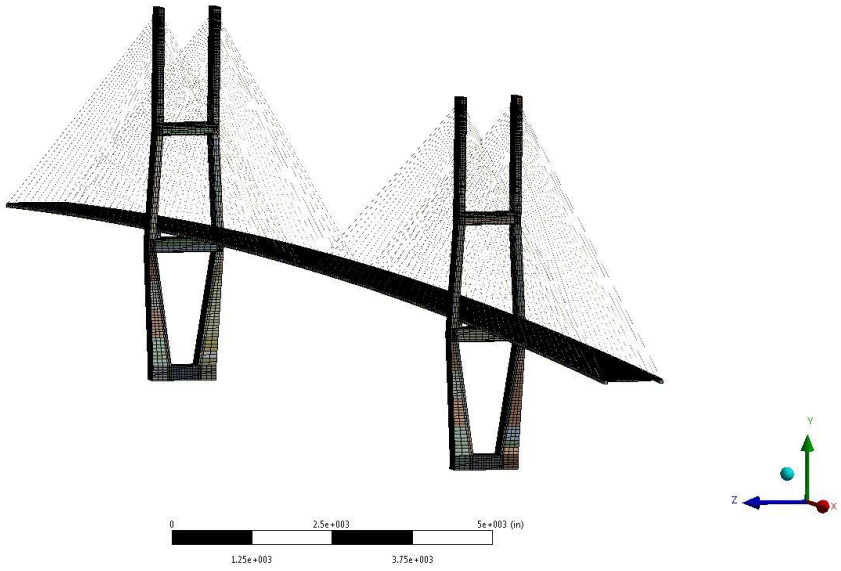

Figure 16 - Sidney Lanier Bridge Fully Meshed

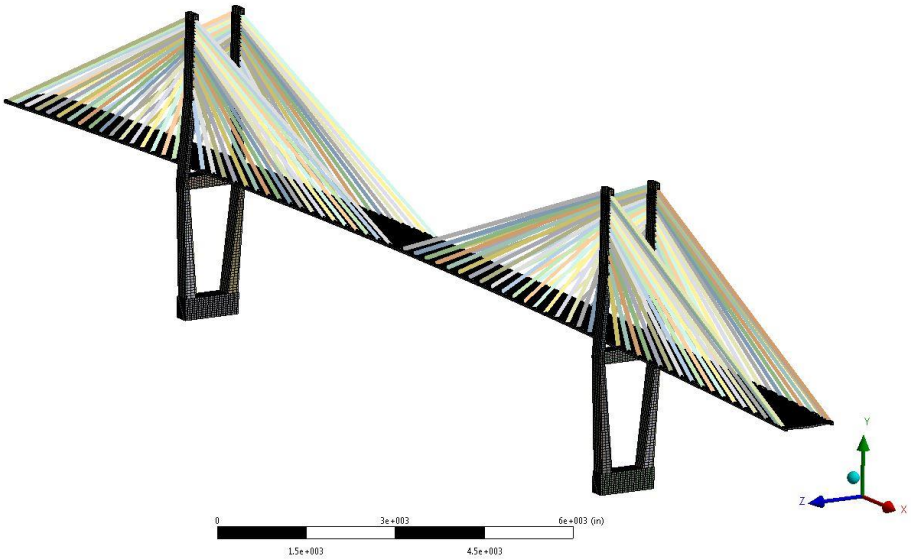

Figure 17 - Eugene Talmadge Memorial Bridge Fully Meshed

2.3.7 Conclusions

Within this finite element model, four different elements were used: solid185, solid186, beam188, and link10. All of the elements other than link10 are cubic elements, which improved solution accuracy compared tetrahedron elements.

2.4 Assignment of Connections

To construct a component based finite element model within ANSYS 16.2 Workbench software requires the use of contact elements which can be either an auto-generated connection or a user generated connection. Four different connection types are used: bonded, fixed, general, and no separation. The purpose of these connections is to ensure a degree of compatibility between adjacent elements along boundaries.

The bonded connection constraint can be applied to edges, surface, and bodies. Within the cable-stayed bridge model this is an automatically generated connection and is used to constrain two coincident surfaces together. Primarily these connections are located within the tower between the tower legs and cross-ties.

The fixed joint connection is primarily used for joining cables to the decks and towers. This joint type constrains all six degrees of freedom.

The general joint enables the user to decide which of the six degrees of freedom are constrained. This joint has been applied between the tower and the concrete block to which the deck connects.

The no separation joint forces and equal amount of displacement between two components. This joint was used to represent the elastomeric bearing connection between the tower and deck.

All of these connections and joint types allow for nodes within a specified distance from a point to be constrained similarly. This is called a pinball area and is used for the cables and tower

deck connections to ensure that the nodes outside of the pinball are not over constrained. The user should check all joints to ensure that the constraints are correct and any auto-generated joints are disabled.

2.5 Assignment of Material Properties

The bridge structure consists of a segmental post-tensioned concrete deck, two concrete towers, and high strength steel cable stays which connect the deck to the towers. The concrete is reinforced with mild steel reinforcement and post-tensioning tendons. The tendons are grouted to ensure the bond between concrete and steel and to reduce corrosion in the tendon. The properties of these materials needed for linear structural analysis are density, Young's modulus, and Poisson's ratio.

The deck and towers are composite structures made of steel and concrete. A simplified approach commonly used in linear analysis is to smear the steel properties over the volume of the concrete. The effect of the steel on the modulus and Poisson's is typically ignored. The density for dynamic analysis must be increased because steel is much denser than concrete.

2.5.1 Concrete

Concrete as a material has a variable density dependent on the mixture of the five materials which make up the concrete matrix: air, rock, water, sand, and cement. Furthermore, to improve concrete's performance, supplementary cementitious material may at times be added to the mixture to help the material acquire desired characteristics. The density of concrete is an important element in the overall analysis as it is the property used in multiple different analyses from a static analysis to the calculation of overall deadweight of the structure.

For a dynamic analysis, the density is used to define mass matrixes that are involved with a modal analysis. Within both cable-stayed bridge documentation, the specified unit weight in pounds per cubic foot are noted and can be seen below in Table 2. All of the units weight specified include the weight of steel reinforcement.

Table 2 - Specified Density of Concrete Components

Georgia Department of Transportation Specified Densities		
Eugene Talmadge Memorial Cable-Stayed Bridge		
Seal	2322 (145)	$\frac{kg}{m^3}$(pcf)
Footing	2402 (150)	$\frac{kg}{m^3}$(pcf)
Parapet & Median Barrier	2402 (150)	$\frac{kg}{m^3}$(pcf)
Deck & Tower	2402 (150)	$\frac{kg}{m^3}$(pcf)
Cable Grout	2002 (125)	$\frac{kg}{m^3}$(pcf)
Sidney Lanier Cable Stayed Bridge		
Seal	2322 (145)	$\frac{kg}{m^3}$(pcf)
Footing	2402 (150)	$\frac{kg}{m^3}$(pcf)
Parapet & Median Barrier	2402 (150)	$\frac{kg}{m^3}$(pcf)
Deck & Tower	2402 (150)	$\frac{kg}{m^3}$(pcf)
Cable Grout	2002 (125)	$\frac{kg}{m^3}$(pcf)

2.5.2 Compressive Strength

Because concrete is not a singular material but a matrix of multiple different constituents, the compressive strength for material can vary depending on the desired strength of the component. The verification of compressive strength is detailed within ASTM (American Standard for Testing Materials) C39. Georgia DOT specifies required compressive strengths for various structural components as shown in Table 3.

Table 3 - Specified Compressive Strength's for Concrete Components..

Georgia Department of Transportation Specified Compressive Strength's			
Eugene Talmadge Memorial Cable-Stayed Bridge			
Component	Class	Compressive Strength	
Deck & Floor Beams & Edge Girder	AAA	263 (5500)	kPa (psf)
Tower	AAA	239 (5000)	kPa (psf)
End Pier	AA-1	191 (4000)	kPa (psf)
Foundation	AA-1	191 (4000)	kPa (psf)
Seal	A	144 (3000)	kPa (psf)
Parapet	AA	166 (3500)	kPa (psf)
Sidney Lanier Cable Stayed Bridge			
Deck & Floor Beams & Edge Girder	AAA	263 (5500)	kPa (psf)
Tower	AAA	239 (5000)	kPa (psf)
Anchor Pier	AA-1	215 (4500)	kPa (psf)
Foundation & Plinth	AA-1	215 (4500)	kPa (psf)
Seal	A	144 (3000)	kPa (psf)
Parapet & Median Barrier	AA	166 (3500)	kPa (psf)
Caissons	AA-1	215 (4500)	kPa (psf)

2.5.3 Young's Modulus

American Concrete Institute (ACI) 318-14 code provides an equation for computing Young's modulus based on the compressive strength as follows:

$$E_c = 57000\sqrt{f_c'} \quad (in\ psi, f_c' < 6000psi) \tag{1}$$

where E_c is the modulus of elasticity and f_c' is the 28 day compressive strength of the concrete. It should be noted that this equation only holds true for concrete of a compressive strength of less than 41.4 MPa (6000 psi), and that all numbers entered and produced are in the units of psi.

2.5.4 Poisson Ratio

The Poisson ratio is the engineering property that defines the relationship between lateral strain and vertical strain and helps define a concrete linear-elastic relationship. Typical values for concrete range between 0.11 to 0.22. This model uses a ratio of 0.2.

2.6 Post Tensioning

Within the Eugene Talmadge and Sidney Lanier bridges, there are multiple forms of post-tensioned structural components. These components are the transverse beams, the bridge deck, the cross-ties within the tower, and the cables. Post-tensioning is the process of running multiple extruded steel wires which are grouped together in tendons, through a concrete section. Blocking off one end of (or anchoring) these tendons and then jacking the other end of the tendons to a specified strain such that the appropriate stress level is reached.

The tendons are placed within the concrete structure and are sheathed within plastic piping (or ducts) so that they do not bond to the concrete. The post-tensioning tendons can have multiple effects on a structure. First, with regards to concrete, they place a large compressive force on the

concrete. This coupled with the tendons location within the section can cause a large internal moment to be formed thereby enabling the concrete structure to better withstand forces before reaching a cracked state. Secondly, when a structure is not built as one continuous section, these tendons can tie all of the separate sections together allowing for moments to translate throughout the whole section. Finally, with, the post tensioning cables that are constructed of multiple tendons enables alteration of the cable-stayed bridges initial deflected shape.

2.6.1 Material Properties

The post tensioning tendons are specified to be of 0.6 in diameter low relaxation grade 270 steel. With a yield strength of 1862 Mpa (270 ksi) a Young's modulus of 1.93E5 MPa (28,000 ksi), and a Wobbles coefficient of 6.56E-3 rad/m (0.0002 radians/ft). The Wobbles coefficient informs the amount of allowable losses due to poor workmanship of the duct within which the tendons are resting.

2.6.2 Application by Means of Thermal Stresses

, There are multiple different methods to apply these post-tensioning loads to a model within ANSYS. The chosen form for applying the post-tensioned loads to different structural components is through the use of thermal loading. This is done through the relationship of strain and heat capacity using the following equation.

$$\epsilon = \alpha \Delta T \qquad (2)$$

where ϵ is the strain, α is the heat capacity of the material, and ΔT is the overall change in temperature. Within the construction documents, the required stressing of the tendons is known, and the Young's modulus for each material is also known, using Hooke's law the strain in the material can be calculated. The required change of temperature within a structural component can

be determined allowing one to apply either an expansion or contraction force within the component.

2.6.3 Continuity Tendons Stress Analysis

There are a total of 38 strands made up of 4 seven wire tendons placed within the 11in thick portion of the main span of the bridge deck for the Sidney Lanier bridge. With each tendon being jacked to a force of 832 kN (187 kips) placing a total force of 3327 kN (748 kips) per strand, an overall compressive force of 1.26E5 kN (28,424 kips) is placed across the bridge deck section. The overall stress placed on this section is then 23.3 MPa (3.385 ksi) since the 0.279 m (11in) thick portion of the deck has an overall area of 5.49 m^2 (8514 in^2). Using a pre/post tension analysis using Eq. 3 on the bridge deck section, the pre-stress force on the top portion of the deck is determined to be 273.1 MPa (39.61 ksi).

$$\sigma = \frac{fey_t}{I} \tag{3}$$

where σ is the developed stress, f is the total jacking force applied to the tendons, e is the distance of the tendons from the centroid of the section, y_t, is the distance of the top of the deck to the centroid of a bridge deck section. This is then combined with the overall compressive force placed on the section of 23.4 MPa (3.39 ksi) to yield a total 296.4 MPa (42.99 ksi) of compressive stress on the top of main span portion of the deck.

This process was repeated for the side spans of the Sidney Lanier bridge. It has 34 total strands with each strand being made up of 4 seven wire tendons. These tendons have been likewise jacked to a force of 832 kN (187 kips) per tendons and thus yields a total force of 3327 kN (748 kips) per strand. Enabling a force of 1.13E5 kN (25,432 kips) to be placed on the side span sections of the bridge. The two resulting stresses are 20.60 MPa (2.987 ksi) in compressive stress and 244.3

MPa (35.43 ksi) in pre-stressing forces, providing a total of 264.9 MPa (38.42 ksi) in compressive stress on the top of the side span portions of the deck.

Determining the stresses placed on the section due to pre/post-tensioning forces, the overall strain for both the main and side spans is calculated using Hooke's law with these being 0.00988 and 0.00883 mm/mm (in/in), respectively. Having calculated the strain, the required differential temperature needed to place this strain on the section is determined by using Equation 2-2 shown above. This provides a needed change in temperature of 805.6 and 718.1 Celsius (1482.1 and 1324.6 degrees Fahrenheit), respectively. Because the post tensioning forces are placing the deck in compression, the change in temperature must be signed negatively to place the material in contraction.

2.6.4 Application of Calculated Strains

Having determined the needed temperature for applying the appropriate strain within the concrete section, there are two ways for applying these thermal loads with ANSYS 16.2 Workbench. These loads are applied either as a body or surface temperature load. Each type has a specific application. A complete change in body temperature is appropriate if an internal bending moment within the section is unwanted. While a surface load is appropriate, if an internal bending moment is wanted within the section for this specific application, a surface temperature was applied to the top and bottom of the deck to develop the internal bending moment. Selection of these surfaces can be seen in Fig. 18 below.

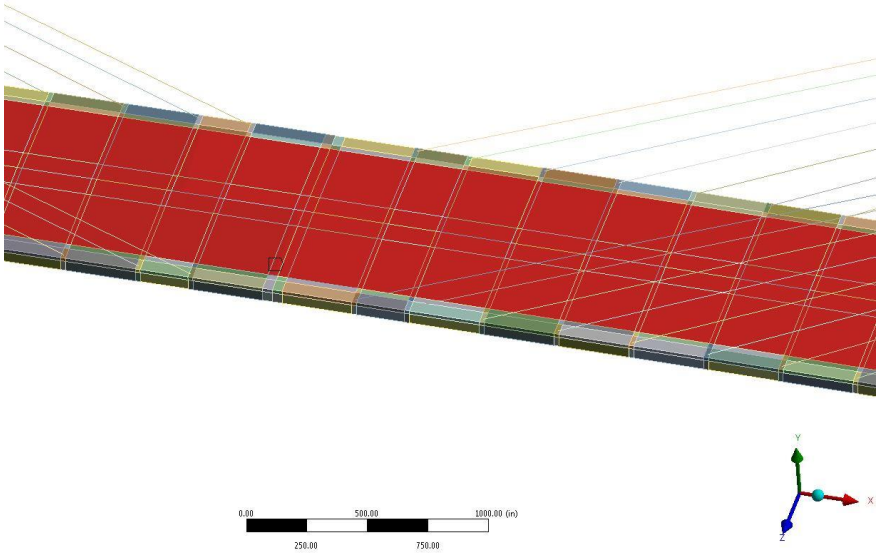

Figure 18 - Selection of Top of Deck Surface for Thermal Strains

2.6.5 Transverse Beam Stress Analysis

Within each of the transverse beams running underneath the deck of Sidney Lanier bridges, there are 219 strand tendons each having an applied jacking force of 3959.0 kN (890 kips), and thus, a total post tension force of 7917.8 kN (1,780 kips) is applied to the section. This places a compressive force of 6.96 MPa (1.01 ksi) across the section, along with pre/post tension force of 21.44 MPa (3.11 ksi) on the section, and finally a dead load internal stress of.0337 MPa (0.00489 ksi) is applied. This places the top in compression with an overall stress of 14.48 MPa (2.10 ksi), and the bottom the beam in tension with a stress of 28.41MPa (4.12 ksi). The strains are 0.00048 4.80×10^{-4} in/in and 9.40×10^{-4} in/in, respectively, providing a needed change in temperature of 22.22 and 61.13 Celsius (71.99 and 142.03 degrees Fahrenheit), respectively.

2.6.6 Application of Calculated Stresses

These changes in temperature were applied to the model in the form of surface temperatures in order to develop the internal bending moment within the transverse beam. Furthermore, because

the top of the beam is in compression, the temperature has been signed negatively to cause a contraction of the concrete. Whereas the bottom of the beam is in tension, the change in temperature has been signed positively to cause the appropriate expansion within the material.

2.6.7 Accounting for Losses

Within post-tension construction the loss of stress provided by post-tension tendons must be accounted for. The losses occur due to elastic shortening of the strand, relaxation of the stand, shrinkage, and creep of the concrete. A conservative estimate of 20% is being taken on the jacking force for the losses seen within the post tensioned sections.

2.6.8 Cable Stress Analysis and Applied Post-Tensioning

The construction documents provided the jacking force applied to each individual cable. The jacking stress was divided by the overall area of steel in the cable in order to determine the internal stress of the cable. Using the Hooke's law, the internal strain of the cable was calculated, and thus providing the overall change in temperature needed to be applied to determine the correct stress. This was completed for each cable individually by applying the total change in body temperature within the model.

2.7 Discussion

The goal of creating a hex dominant mesh requires time and an understanding of the overall cable-stayed bridge structure. The structure could have been meshed with different element types; however, due to the desired behavior, it has been chosen not to. Convergence of each individual component was checked to ensure the results are correct. This is necessary within any FEA analysis. Material properties play an important role in defining the global behavior of the structure. They have been assigned accordingly to the specified values within the construction documents.

The post-tensioning of the structure has a global effect on the overall initial stress distribution of the structure and provides sectional capacity to deformation, and the point at which it reaches plastic deformation.

2.8 Conclusion

Meshing, the assignment of material properties, and the application of in-situ stressing of the structural components has been discussed in regards to the two FEA models used within this project. Refinement of the mesh must be completed in order to ensure convergence of the solution as well as to reduce the required overall computational power. This combined with the correctly defined theoretical or experimental material properties helps to ensure that the model will adequately represent the response of the bridges. Finally, the application of post-tension forces through thermal loading has been outlined.

3. VERIFICATION AND VALIDATION OF FEA MODELS

3.1 Verification

The verification of finite element analysis models quantifies how well the numerical approximation (i.e. the model) agrees with known mathematical equations and if the computed results observe basic physical laws such as conservation of energy and momentum. The verification of a model is generally completed in multiple different ways. With concern to the Eugene Talmadge and Sidney Lanier cable-stayed bridge models, the verification was performed through the use of a static analysis including the study of gravity and lateral load cases. Total material takeoffs were performed for each model using hand calculations against the gravity load reactions calculated at the base of the two towers.

A cable-stayed bridge is a set of two cantilevered beams which are supported by towers, wherein one side span and half of the main span overall forces are translated to the base of one of the two towers and then to its associated foundation. This may seem as an over simplification but the underlying principal is still present and provides the user a way of roughly estimating through the use of material take-offs and statics, a way of determining the reactions at the base of the tower. This can then be used to verify the model.

3.2 Method for Checking Model Compatibility

Ensuring that an overall model and components are behaving accurately is important and can be done through many different means. Within this study, the use of static deflected shapes

was used to ensure the correct behavior of the overall structure and the components. Each component was tested within separate static analysis and as a whole. During this static analysis, only gravity loading forces were placed on the models. By applying only gravity loads, the load path of the forces and the behavior can be easily checked and ensured that the forces are traveling appropriately. The base of the two towers are fixed for this verification.

Analyzing the global behavior of the tower as singular structural component, it would be expected that the tower should experience no torsional deflection or out of plane bending and the stress at the top of the tower should be minimal with the stresses gradually building as one travels down the tower and reach a peak stress at the foundation. There should be bowing out of the middle and lower tower legs due to their skewed angles. There should be local points of high stress at the edges of the lower cross-tie working to restrain the bowing out of the aforementioned legs.

The tower as a part of the whole model will behave differently than as singular component. As before, the tower should see minimal stress levels at the top of the tower and build as one moves down the tower and peaking at the foundation. Although, at the top legs, there will be local points of high stress associated with the connections of the cables to the tower. Due to the difference in span weight of the side span and main span, the two towers should experience a moment around the x-axis within one having clockwise rotation and the other a counterclockwise rotation. Both towers should be mirror images of another due to symmetry.

Viewing the deck as a singular component, the developed stress and associated deflected shape are reliant on the support conditions placed on the component. As a singular component, two different support scenarios were placed on the bridge deck. The first constraints were to only restrain the bridge ends in a fixed manner. This type of constraint condition should display an overall deflected shape of the center of the deck reaching maximum deflection with the deflection

smoothly reducing as one travel toward either end. If the deflected shape displays any discontinuities or “pinching”, the geometry and meshing needs to be checked. The second constraint condition placed on the deck was to fix four separate places of the deck. The four locations chosen are both ends, and the two location where the deck runs through the towers. This selection of four constraints on the deck is to ensure the proper behavior under a multiple support condition. The deflected shape should display on the three deflected sections; the largest deflection being the main span of the bridge and the two side spans experience approximately half the deflection of the main span.

When viewing the decks’ behavior within the whole model, there should be localized stress concentrations at site where the cable connects to deck. The overall deflected shape of the deck is the main span and should see maximum deflection and the side spans should experience a slight rise in elevation due to large moment exerted about the tower. Furthermore, there should be slight deflection of the deck between the cables.

The behavior of the cables within a static analysis as singular components needs the constraint of a pinned or fixed condition at either end. Thus, as with the application of a gravity load, the straight line of the cable should deflect into what is known as a catenary curve. This curve should be smooth and not feature any discontinuities. Within relation to the whole model, the cables will be pulled taught due to restraining the dead weight of the bridge deck. The cable should still display a slight catenary curve. The cables should display a uniaxial loading of tension, with the uppermost cables experiencing more stress than the lower cables.

Without understanding the application of first principles within a model and thoroughly verifying/validating the model, the results produced are not trustworthy. Within both the Eugene Talmadge and Sidney Lanier cable-stayed bridge models, each component was verified for

expected load cases, as well as the total reaction forces of the tower from the models. They are compared to those estimated through hand calculations.

3.3 Validation

Validation is the process within numerical modeling concerned with comparing calculated numerical results to those of real-world physical experiments and published literature. This step is a necessary component when performing a numerical simulation due to the fact that theoretical results often differ from experimental results. Furthermore, due to the amount of assumptions made during the modeling process, the validation process helps inform an engineer of the degree of accuracy of the model in relation to it being an accurate representation of real world tests. This validation is best conducted through a comparison of experimental results; however, depending on the scale of the numerical representation, that can prove difficult. This leads engineers to perform component level validations rather than the entire model level validations. Researchers can also look to the literature for published results of similar structures to help ensure the validity of the model.

3.3.1 Modal Analysis

To perform the modal analysis of a cable-stayed bridge, equations of motion for the entire multi-degree of freedom system must first be developed. The overall equation of motion is

$$[m]\{\ddot{u}\} + [c]\{\dot{u}\} + [k]\{u\} = 0, \qquad (3)$$

where [m], [c], and [k] are mass, damping and stiffness matrices and $\{\ddot{u}\}$, $\{\dot{u}\}$, {u} are N by 1 (N represents the number of degrees of freedom of the system) vectors for acceleration, velocity and displacement. For the modal analysis, the undamped unforced equation of motion is considered reducing Eq. (3) to the following form

$$[m]\{a\} + [k]\{u\} = 0 \quad (4)$$

Following this reduction, a solution of simple harmonic nature is then assumed. By allowing Eq. (4) to have a harmonic solution an eigenvalue problem can be produced. The associated harmonic solution and eigenvalue problem are as follows

$$Acos(w_n t) + Bsin(w_n t) = q_n(t), \quad (5)$$

$$([k] - {w_n}^2[m])\{\phi\} = \{0\}, \quad (6)$$

where A and B are constants determined from the initial conditions that originate the motion. The natural frequency is shown via w_n. After substituting Eq. (5) into Eq. (4) and resulting manipulation the associated eigenvalue problem results in Eq. (6), where ϕ is the mode number, ranging from 1 to N. After these manipulations there are two resulting solutions. First is the trivial solution when $\phi = 0$. This solution exhibits that there is no motion within the system of equations. The second solution yields a non-trivial results is when the determinant of Eq. (6) is taken as follows

$$det([k] - {w_n}^2[m]) = 0. \quad (7)$$

By taking the determinant and then expanding it, a polynomial of order N in ${w_n}^2$ is developed. Eq. (7), is then known as the characteristic equation [1] with N real and positive roots for ${w_n}^2$ since the mass and stiffness matrices are symmetric and positive. This above equation can be used to solve for any mode ($\phi = 1,2,3, etc$ ...).

3.3.2 Tool for debugging

Modal analysis is a useful tool for refining model behavior and ensuring that all components are connected. This is due to the fact modal analysis is a dynamic analysis and a cyclic forcing function is used to determine the structure frequencies for natural vibration. In the debugging stage, the deflected shape will identify to the researcher any of the components that are

not attached or if the constraint applied are too weak due to components that are not meshed together. Furthermore, due to the proposed harmonic solution, the deflected shapes of the model should be of a harmonic nature. Enabling the modeler to see a half or full sine or cosine period within the deflected shape, if this is not seen, then it is likely that there is a mistake in subsequent steps and should be addressed.

Within this study, the modal analysis presents itself as a useful tool in performing validation of the Eugene Talmadge Memorial and Sidney Lanier cable-stayed bridges. The two bridges' modal frequencies and deflected shapes have been checked against the wind tunnel documentation provided by Rowan Williams Davis and Irwin Inc (RWDI). Within this documentation the first 20 modes of vibration were identified along with their associated deflected shape. This enabled the two models to be directly compared against the experimental testing performed in the design and construction of these two bridges. Within the wind documentation, RWDI listed the scale factors used and focused on matching width, mass, and mass moment of inertia of their scale model to that of the full scale bridge. Furthermore, validation can be found in the literature by comparing other cable-stayed bridges of similar nature and span lengths.

3.4 Sidney Lanier Cable-Stayed Bridge

The verification of the finite element analysis models is concerned with how well the numerical approximation (i.e. the model) agrees with known mathematical equations and if the computed results observe basic physical laws such as equilibrium and conservation of energy and momentum. The verification of this model was performed through the use of a static analysis. Total material takeoffs were performed for the model using hand calculations and compared to the reaction forces calculated at the base of the two towers due to the gravity load. The vertical reaction force at each tower base is 221,000 kN (49,783 kips). Similar reaction checks were performed for

lateral load cases. The continuity of the elements at cable anchoring points, joints, and bearing connections was reviewed and found satisfactory under static loads.

For the Sidney Lanier bridge, the first 100 modes were determined. From this, it was decided to use only the first twenty modes in subsequent analysis. This was established by investigating the modal participation factors for each mode. It was found that after the twentieth mode, the participation factors decreased to such a point that their contribution was insignificant. The three first major modes for vertical, lateral, and torsional shapes are illustrated in Figs. 19 and 20.

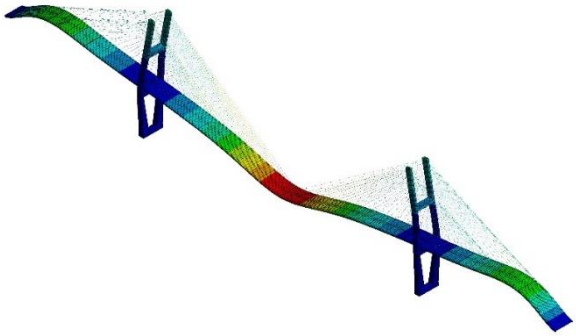

(a) 1st Horizontal mode (Mode 1 – 0.22 Hz)

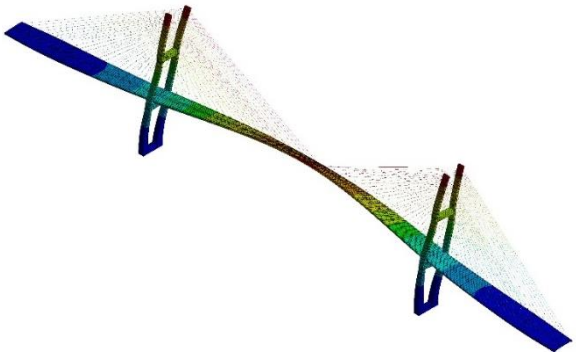

(d) 1st Vertical mode (Mode 3 – 0.317 Hz)

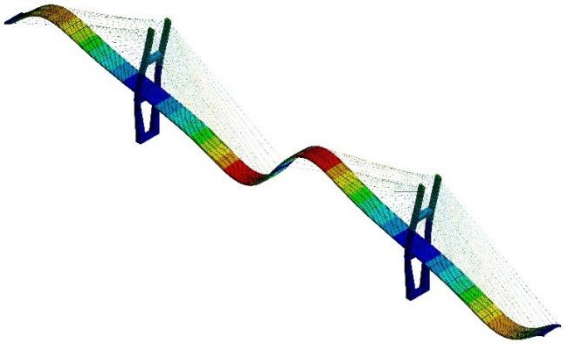

(b) 2nd Horizontal mode (Mode 2 – 0.29 Hz)

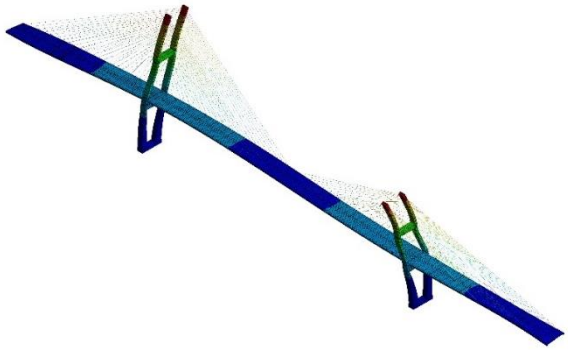

(e) 2nd Vertical mode (Mode 4 – 0.385 Hz)

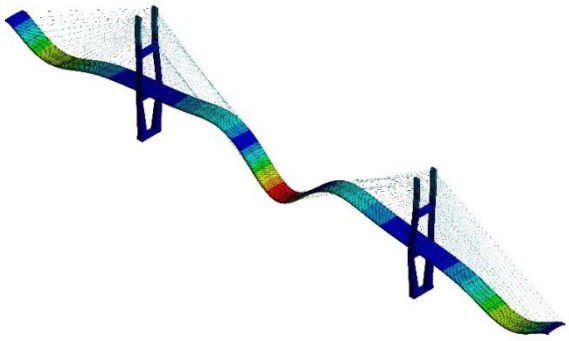

(c) 3rd Horizontal mode (Mode 7 – 0.49 Hz)

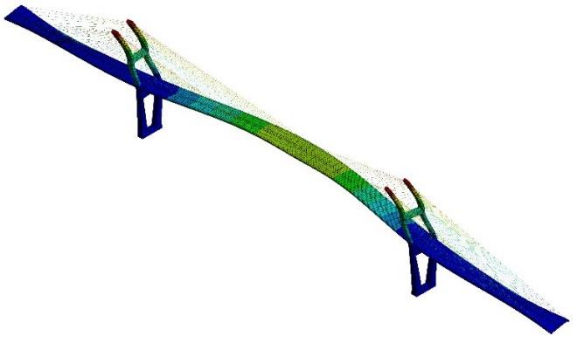

(f) 3rd Vertical mode (Mode 6 – 0.478 Hz)

Figure 19 - Horizontal and Vertical Modes: (a) Mode 1 – 0.22 Hz; (b) Mode 2 – 0.29 Hz; (c) Mode 7 –0.49 Hz; (d) Mode 3 – 0.317 Hz; (e) Mode 4 – 0.385 Hz; (f) Mode 6 – 0.478 Hz (Deformed Shape Display Scale Factor = 23,000).

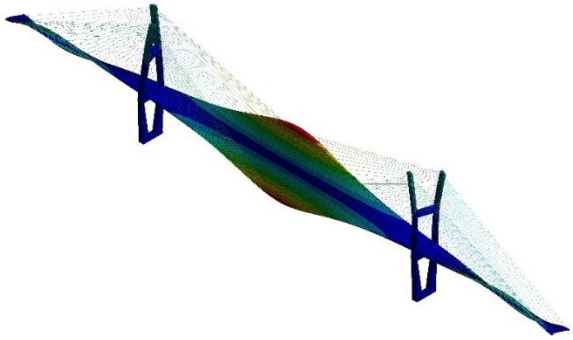

(a) Mode 5 – 0.40 Hz

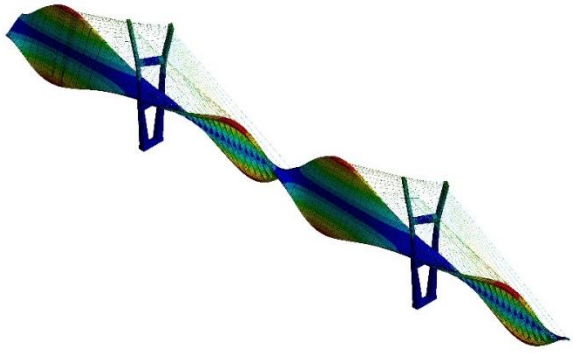

(b) Mode 8 – 0.55 Hz

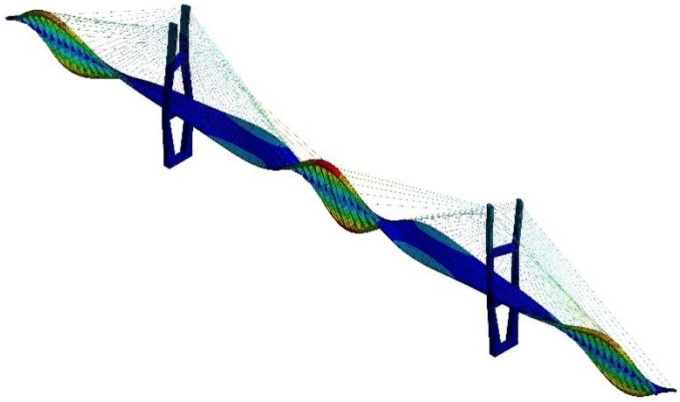

(c) Mode 13 – 0.74 Hz

Figure 20 - Torsional Modes: (a) Mode 5 – 0.40 Hz; (b) Mode 8 – 0.55 Hz; (c) Mode 13 – 0.74 Hz (Deformed Shape Display Scale Factor = 23,000)

Validation is a necessary component when performing a numerical simulation due to the fact that theoretical results often differ from experimental results. Furthermore, due to the assumptions made during the modeling process, the validation process informs the degree of accuracy of the model. This validation is best conducted through a comparison of experimental results. Furthermore, the response of similar structures is studied to ensure the validity of the model.

The wind-induced failure study uses the modal analysis results for validation. The analysis results are compared to those obtained from the design wind tunnel test and modal investigation (RWDI 1997). Within this documentation, the first 20 major modes of vibration are identified along with the bridges associated deflected shapes. This enables direct validation of the model against the experimental testing performed in the design and construction of the bridge. The results obtained in this study are compared to those found within the design-basis wind analysis report documentation (RWDI 1997) and are summarized in Table 4.

Table 4 - Modal Frequency Comparison.

Mode	Analysis Results		Wind Report (RWDI 1997)		% difference in frequencies
	Frequency	Global Shape	Frequency	Global Shape	
1	0.21488	Vertical	0.2530051	1st Vertical	16
2	0.28957	Vertical	0.282253	2nd Vertical	3
3	0.31682	Lateral	0.361494	3rd Vertical (w Long. Motion)	13
4	0.385336	Asym-Lateral	0.439482	1st Lateral	13
5	0.396884	Torsional	0.500188	Tower Lateral	23
6	0.478369	Lateral	0.520963	4th Vertical	9
7	0.485959	Vertical	0.558226	2nd Lateral	14
8	0.54929	Torsional	0.577534	5th Vertical	5
9	0.579666	Vertical	0.635218	6th Vertical	9
10	0.643816	Vertical	0.6947748	3rd Lateral (Mainly Side Span & Tower)	8
11	0.704083	TOWER DOM	0.735437	7th Vertical	4
12	0.704109	TOWER DOM	0.774759	8th Vertical	10
13	0.740928	Torsional	0.795442	9th Vertical	7
14	0.751304	Vertical	0.806402	Tower Lateral	7
15	0.801575	Vertical	0.839677	Tower Lateral	4
16	0.832308	Vertical	0.839964	Tower Lateral	1
17	0.836886	Torsional	0.866226	10th Vertical	3
18	0.854043	Torsional	0.96903	1st Torsional	13
19	0.856572	Torsional	1.013811	11th Vertical	17
20	0.858445	Torsional	1.073017	12th Vertical	22

A slight difference exists between the modal frequencies calculated by this study and those calculated in the wind report. This outcome was attributed to the total mass utilized during the design phase, which was slightly different from the mass calculated based on the complete

construction drawings and thus accounts for the dissimilarity between frequencies. As the total mass was adjusted, the frequencies became nearer to those outlined by the wind report. Finally, as-built conditions including the mass are best reflected in the FEA model.

3.5 Eugene Talmadge Cable-Stayed Bridge

For the Eugene Talmadge bridge, the first 100 modes were determined. From this, it was decided to use only the first twenty modes in subsequent analysis. They were selected by determining the modal participation factors for each mode. It was found that after the twentieth mode, the participation factors decreased to such a point that their contribution was insignificant. The three first major modes for vertical, lateral, and torsional shapes are illustrated in Figs. 21 and 22.

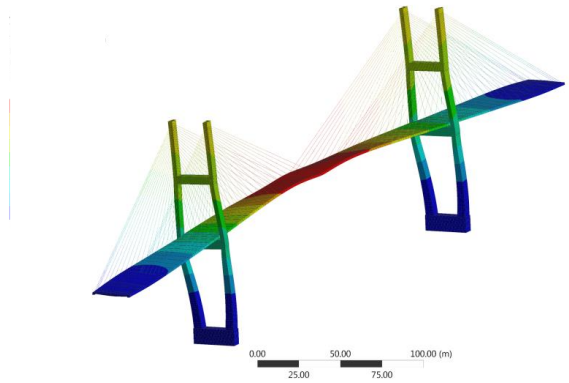

(a) 1st Horizontal mode (Mode 2 – 0.33 Hz)

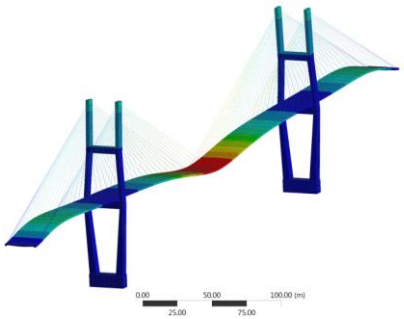

(d) 1st Vertical mode (Mode 1 – 0.27 Hz)

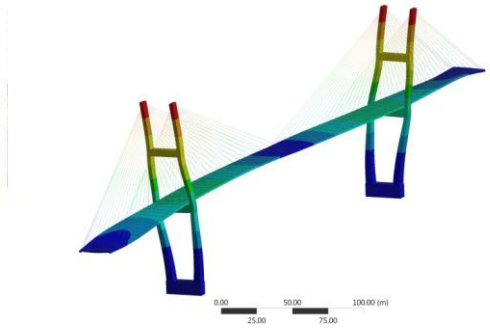

(b) 2nd Horizontal mode (Mode 4 – 0.48 Hz)

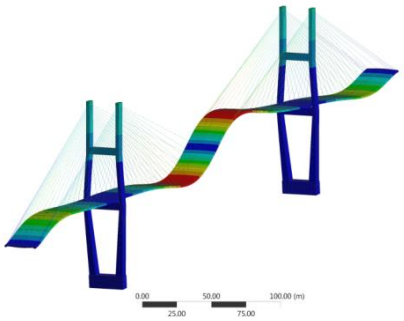

(e) 2nd Vertical mode (Mode 3 – 0.36 Hz)

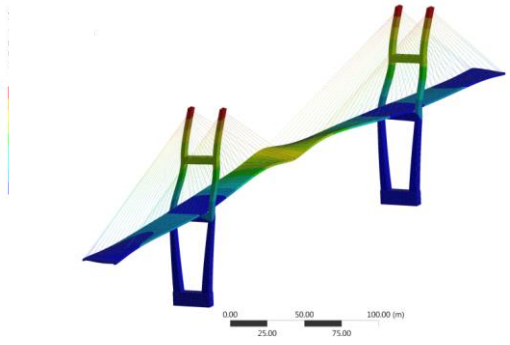

(c) 3rd Horizontal mode (Mode 9 – 0.68 Hz)

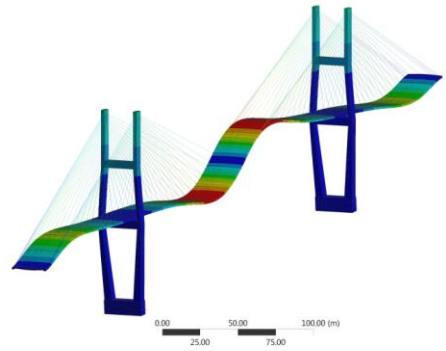

(f) 3rd Vertical mode (Mode 6 – 0.59 Hz)

Figure 21 - Horizontal and Vertical Modes: (a) Mode 2 – 0.33 Hz; (b) Mode 4 – 0.48 Hz; (c) Mode 9 –0.68 Hz; (d) Mode 1 – 0.27 Hz; (e) Mode 3 – 0.36 Hz; (f) Mode 6 – 0.59 Hz (Deformed Shape Display Scale Factor = 23,000).

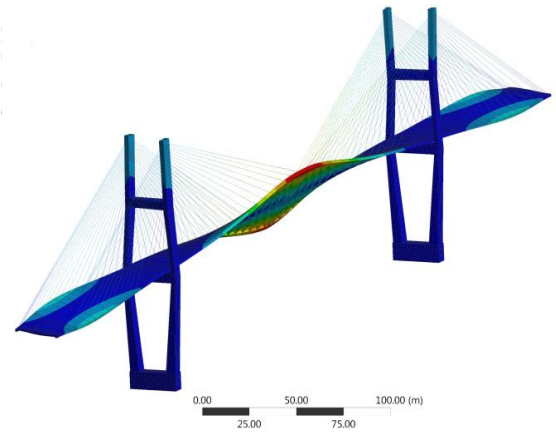

(a) Mode 5 – 0.48 Hz

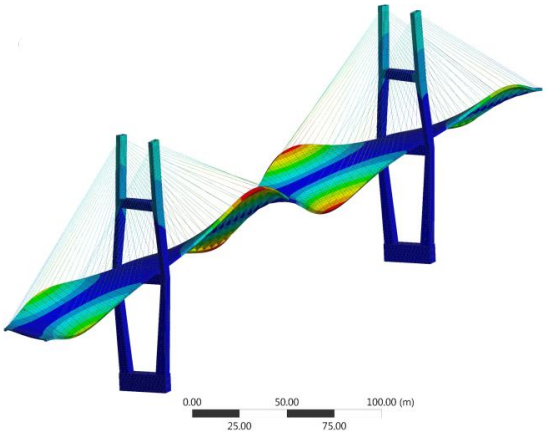

(b) Mode 8 – 0.67 Hz

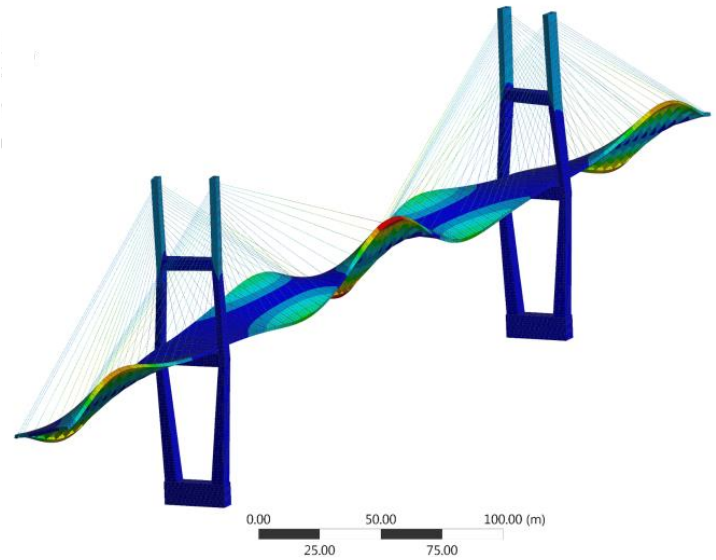

(c) Mode 12 – 0.90 Hz

Figure 22 - Torsional Modes: (a) Mode 5 – 0.48 Hz; (b) Mode 8 – 0.67 Hz; (c) Mode 13 – 0.90 Hz (Deformed Shape Display Scale Factor = 23,000).

The wind-induced failure analysis study used the modal analysis results for validation. The analysis results were compared to those obtained from the design wind tunnel test and modal investigation (RWDI 1997). Within this documentation, only selected modes of vibration were

identified along with the bridges associated deflected shapes. This enabled the model to be directly validated against the experimental testing performed in the design and construction of the bridge. The results of the analytical results obtained in this study were compared to those found within the design-basis wind analysis report documentation (RWDI 1997) and are summarized in Table 5. Similar to the Sydney Lanier bridge, a slight difference exists between the modal frequencies calculated by this study and those calculated in the wind report. As the total mass was adjusted, the frequencies became nearer to those outlined by the wind report. The frequencies becoming nearer those outlined by RWDI can be seen in the modal information provided by RWDI for their construction stage evaluation of the Talmadge bridge. This provided further validation to the overall analytical model, this can be seen in Table 6. Within the FEA model the mass and stiffness of the materials were adjusted to be a closure representation of the RWDI documentation. From Table 6 the frequencies are seen to be close. As well as the displaced shapes are the same.

Table 5 - Modal Frequency Comparison.

Mode	Analysis Results		Wind Report (RWDI 1997)		% difference in frequencies
	Frequency	Global Shape	Frequency	Global Shape	
1	0.2706	Vertical	0.222	Vertical	19
2	0.3285	Lateral	0.274	Lateral	18
3	0.3260	Vertical	Not Avl.	Not Avl.	Not Avl.
4	0.4800	Lateral	Not Avl.	Not Avl.	Not Avl.
5	0.4834	Torsional	Not Avl.	Not Avl.	Not Avl.
6	0.5688	Vertical	Not Avl.	Not Avl.	Not Avl.
7	0.6728	Vertical	Not Avl.	Not Avl.	Not Avl.
8	0.6738	Torsional	Not Avl.	Not Avl.	Not Avl.
9	0.6764	Lateral	Not Avl.	Not Avl.	Not Avl.
10	0.7322	Vertical	Not Avl.	Not Avl.	Not Avl.
11	0.8454	Vertical	Not Avl.	Not Avl.	Not Avl.
12	0.8986	Torsional	Not Avl.	Not Avl.	Not Avl.
13	0.9735	Vertical	Not Avl.	Not Avl.	Not Avl.
14	1.0036	Torsional	Not Avl.	Not Avl.	Not Avl.
15	1.0379	Vertical	Not Avl.	Not Avl.	Not Avl.
16	1.0710	Vertical	Not Avl.	Not Avl.	Not Avl.
17	1.0790	Torsional	Not Avl.	Not Avl.	Not Avl.
18	1.0927	Lateral	Not Avl.	Not Avl.	Not Avl.
19	1.1624	Vertical	Not Avl.	Not Avl.	Not Avl.
20	1.1731	Tower Dominant	Not Avl.	Not Avl.	Not Avl.

Table 6 – Construction Stage Validation.

Eugene Talmadge Memorial Validation						
Construction Stage		FEA Model		RWDI Documentation		Percent Diff. (%)
	Mode	Frequency	Shape	Frequency	Shape	
23	1	0.272	Vertical	0.262	Vertical	3.75
	2	0.582	Torsional	0.624	Torsional	6.97
27	1	0.211	Vertical	0.222	Vertical	5.08
	2	0.28	Torsional	0.274	Torsional	2.17

While the bridges frequencies of the FEA model can be matched through the adjustment of mass and stiffness to that of RWDI provided information. It is felt that the data provided within the construction documentation is more appropriate and better represents the in-situ condition of the bridge.

4. ANALYSIS PROCEDURE AND RESULTS

4.1 Sidney Lanier Analysis and Results

This section quantifies the types of wind loads investigated and how wind forces are applied to the bridge structure under investigation as they represent the static and dynamic effects of wind on the bridge. The dynamic wind loads are generally considered in terms of an equivalent static wind load. The demand and capacity of the cable-stayed bridge structure are determined for each component of growing wind speeds associated with hurricanes of different strength. Vehicular loads are not included in the analysis because the bridge is assumed to be closed during storm events.

Table 7 - Wind Speed and Hurricane Categories.

	Minimum		Maximum	
Categories	m/s	mph	m/s	mph
1	42.5	95	42.5	95
2	49.2	110	49.2	110
3	57.7	129	57.7	129
4	69.7	156	69.7	156
5	70.2	157	70.2	n/a

The wind speeds are evaluated based on the Stafford-Simpson Wind Speed scale of 1 minute sustained wind loading as shown in Table 7. Within this study, the Sidney Lanier cable-stayed bridge was evaluated for the three major deformation and/or failure patterns: a lift (vertical) force, drag (lateral) force, or a pitch (torsion). A visual representation of these global bridge response patterns is shown in Figs. 23 and 24. These dynamic contributions of the bridge behavior are translated into forces through an equivalent static loading pattern, which is denoted as F_d in

Eq. (3), where F_T, F_s, and F_d is the total, static, and dynamic force, respectively. Eq. (8) provides the total force to be applied across the bridge structure for each of the three failure patterns.

$$F_T = F_s + F_d \tag{8}$$

4.1.2 Determination of Static Wind Pressure

The static force, F_s, components (F_{sd}, F_{sl}, and M_{sp}) are determined by aerodynamic force equations for lift, drag, and pitch, as shown in Eqs. (9) through (11), where ρ is the density of the air, *u* is the velocity of the wind, *d* is the depth of the deck or diameter of cables, *B* is the width of the deck, *T* is the thickness of the tower. The coefficients C_x, C_z, C_m are non-dimensional numbers experimentally derived from wind tunnel testing. These provide aerodynamic efficiency of the shape to the engineer. The lateral, vertical, torsional forces on the bridge deck are determined by Eq. (4), (5), and (6), respectively.

$$Lateral\ Force: F_{sd} = \frac{1}{2}\rho u^2 d C_x \tag{9}$$

$$Vertical\ Force: F_{sl} = \frac{1}{2}\rho u^2 B C_z \tag{10}$$

$$Torsional\ Moment: M_{sp} = \frac{1}{2}\rho u^2 B^2 C_m \tag{11}$$

Furthermore, the lateral load on the tower and cables is determined by Eq. (12) and (13), respectively.

$$Lateral\ Force\ Tower: F_{sl\_tower} = \frac{1}{2}\rho u^2 T C_x \tag{12}$$

$$Lateral\ Force\ Cables: \quad F_{sl\_cables} = \frac{1}{2}\rho u^2 d C_x \tag{13}$$

4.1.3 Determination of Dynamic Wind Effects

The dynamic component, F_d, of the total force is broken down further into two different components as shown in Eq. (14). To ensure accurate representation of all forces on the bridge, a

root-mean-square normalization is performed, ultimately enabling all contributions of dynamic force to be represented equally, where U is a dynamic factor applied to the static force (F_s) enabling the dynamic term to become wind speed dependent (RWDI 1997).

$$F_d = \sqrt{(UF_s)^2 + (\sum_{j=1}^{n} F_m)^2} \tag{14}$$

The second term, F_m, within Eq. (9) is determined by Eqs. (15) through (17) and is the equivalent static force to represent the dynamic wind effects on the bridge under different frequencies capable of occurring due to wind loading. 'n' denotes total number of modes used for the analysis. Only pertinent modes are selected for each of three load cases vertical, lateral, and torsional (F_v, F_h, and M).

This term takes the modal frequencies, modal deflected shapes, and mass per node and converts it to a force as shown in Eqs. (15) through (16), where m is the mass per node, I_m is the mass moment of inertia per node, N_j is the jth modal frequency in Hz, Z_j is the jth peak value of the modal deflection, and theta, θ_j, is the jth mode shape. This process is illustrated through an example shown later.

$$\left[F_{v_j}\right] = \left(2\pi N_j\right)^2 m[Z_j][\theta_j] \tag{15}$$

$$[F_{h_j}] = \left(2\pi N_j\right)^2 m[Z_j][\theta_j] \tag{16}$$

$$[M_j] = \left(2\pi N_j\right)^2 I_m[Z_j][\theta_j] \tag{17}$$

Each mode within the first twenty modes is summarized in Table 1 and was reviewed to determine if the overall displaced shape fell within a vertical, lateral, or torsional case. Subsequently, the above equations were applied to determine equivalent static forces (F_v, F_h, and M) for that specific mode.

These derived forces were applied to the bridge deck, bridge towers, and bridge cables. The static lift, pitch, and drag forces were applied as surface pressure to associated geometries and are illustrated in Figs. 23(a) and 24(a). While the static pitch, (moment) was applied by a moment-couple on either side of the bridge deck to achieve a torsional behavior. Figs. 25(a) through 25(c) present the deformed shape resulting from static lift, drag, and pitch cases, respectively. Furthermore, lateral pressure was applied to the cable (or beam) elements, as well as the towers. The dynamic portion of loading was applied as nodal forces as illustrated in Fig. 23 and 24. In the case of the static forces for lift and drag, a pressure load was used within the modeling software. This allowed for the pre-determined pressure to be applied across the selected surface for lift and drag. A unit load of force per unit length was used for the 'pitch' case since couples were used in representing the torsional displacement. In Figs. 23(b) and 24(b), "U" multiplies the static portion a coefficient that enables the static to become dependent on wind speed. Although the magnitude of the dynamic forces is determined by Eq. (9), the force patterns need to be consistent with the mode shapes. Therefore, the first 20 mode shapes were exported at pre-selected nodes for vertical and torsional modes and were imported to apply the dynamic force patterns for a modal superposition. In the lateral case, a single line of nodes on one side was utilized due to the symmetric geometry. This mode shape (or normalized deformation) data was then translated into force patterns by utilizing the nodal mass. The mode shapes were exported from the modal analysis results and operated using Eqs. (10) through (12) to determine nodal forces. The FEA model determines the force distribution from the linear elastic analysis. Utilizing the internal forces determined from the analysis, a cracked section analysis was considered without redistributing the loads. After reviewing the principal stresses, it was determined that this 'cracked' section assumption is reasonable for beyond design-basis wind load cases.

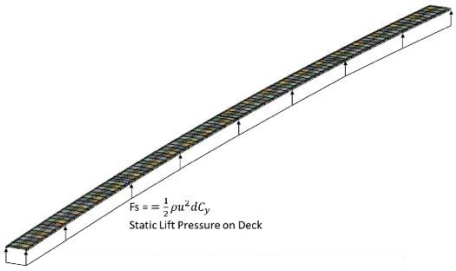

(a) Static Wind Load

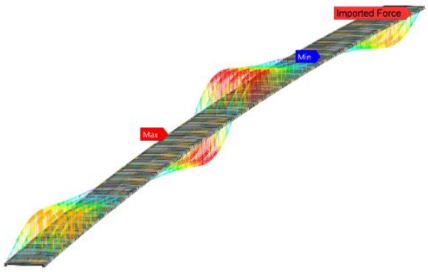

(d) Load Reflecting 2nd Vertical Mode

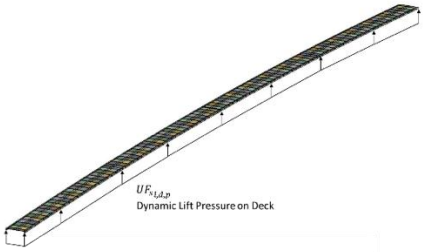

(b) Dynamic Load as a constant function of Static Load

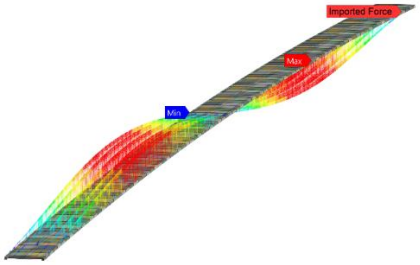

(e) Load Reflecting 3rd Vertical Mode

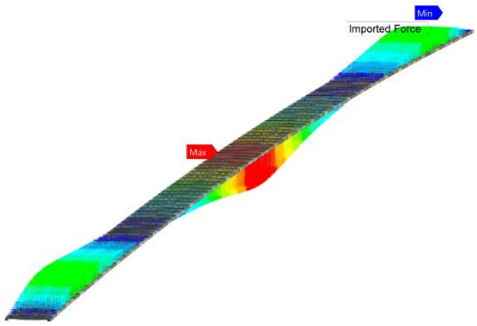

(c) Load Reflecting 1st Vertical Mode

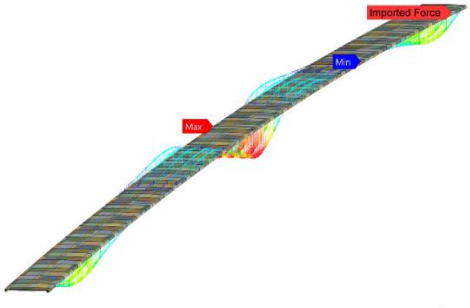

(f) Load Reflecting 4th Vertical Mode

Figure 23 - Static and Equivalent Static Vertical Wind Load Patterns to Account for Dynamic Wind Load: (a) Static wind load; (b) Dynamic Load as a constant function of the static load; (c) Dynamic Load Patterns from the first; (d) Second; (e) Third; (f) Fourth vertical mode shapes

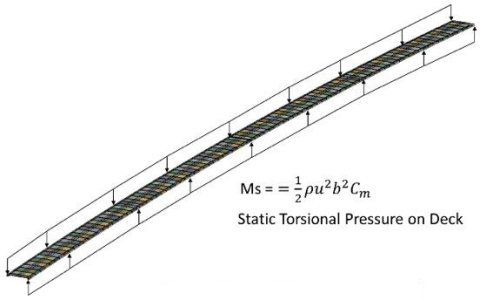

(a) Static Wind Load

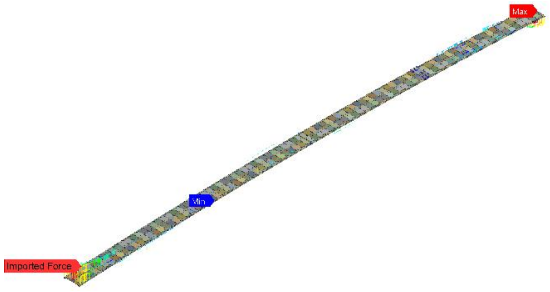

(d) Load Reflecting 2nd Torsional Mode

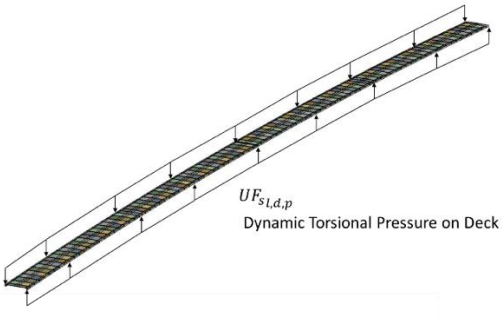

(b) Dynamic Load as a constant function of Static Load

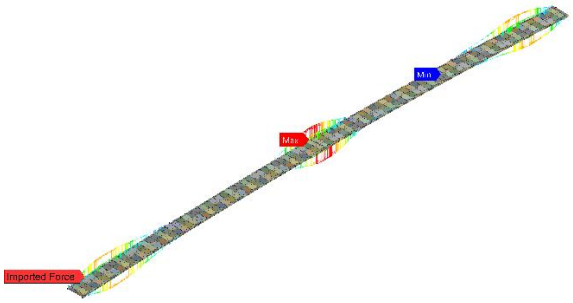

(e) Load Reflecting 2nd Torsional Mode

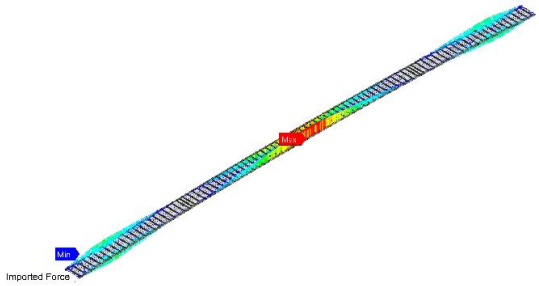

(c) Load Reflecting 1st Torsional Mode

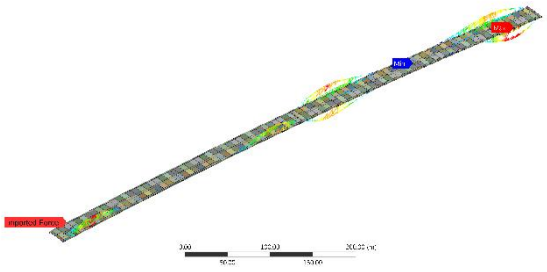

(f) Load Reflecting 4th Torsional Mode

Figure 24 - Static and Equivalent Static Vertical Wind Load Patterns to Account for Dynamic Wind Load: (a) Static wind load; (b) Dynamic Load as a constant function of the static load; (c) Dynamic Load Patterns from the first; (d) Second; (e) Third; (f) Fourth torsional mode shapes.

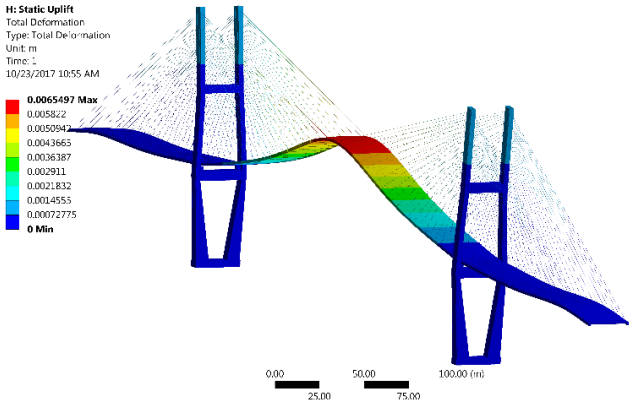

(a) Vertical Deformation (m) for Static Vertical Wind Load

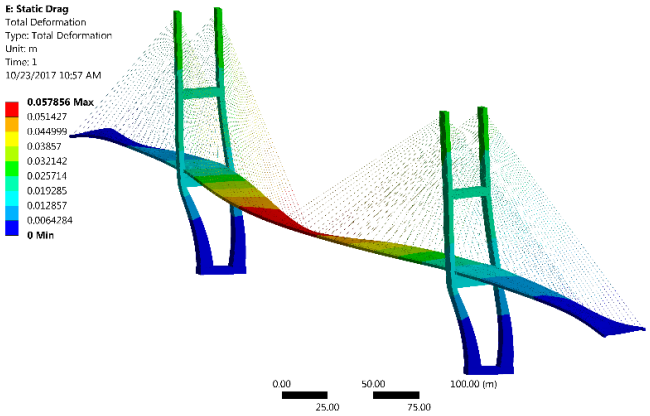

(b) Lateral Deformation (m) for Static Lateral Wind Load

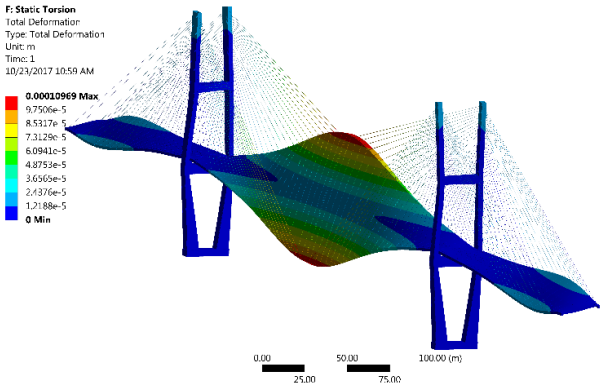

(c) Total Deformation (m) for Static Torsional Wind Load

Figure 25 - Deformation of the Model for Static Wind Load Cases. (Deformation Display Scale Factor =30,000)

The nodal forces were applied as imported loads on the pre-selected nodes in the ANSYS mechanical software version 16.2. Figs. 23(c) through 23(f) illustrate the nodal forces applied to the bridge deck to account for dynamic effects from the vertical wind load case. Figs. 24(c) through 24(f) illustrate the asymmetric nodal forces applied to the bridge deck to account for dynamic effects from the torsional wind load case. The lateral case is applied in similar manner to that of the vertical and torsional cases.

4.1.4 Internal Force Demand by Static and Dynamic Wind Loads

It is important to first define the meaning behind the word "demand" as it is being used in this paper. The force demand represents internal forces determined by performing a linear elastic analysis of the FEA model for the static and equivalent wind load cases. Within this wind analysis, the force demand is determined as internal force demand placed on each element or combination of elements due to the combined static and dynamic wind forces.

4.1.5 Capacity of the Bridge Components

The "capacity" being considered refers to the stress levels necessary within the bridge section to cause yielding of the tensioned steel within the reinforced concrete section and thus does not necessarily represent the ultimate strength of deck and tower sections. That would require a thorough review of the design and construction documents of the structure including the layout and grade of the reinforcing steel.

Three sections within the bridge deck were identified: the slab, edge beam, and transverse floor beam. Four sections within the tower were identified: the lower tower section of the tower directly above the plinth; the lower tower section of the tower directly below the first tower cross-

tie, the middle of the middle tower leg, and finally, the middle of the top tower leg. These sections are illustrated in Fig. 26.

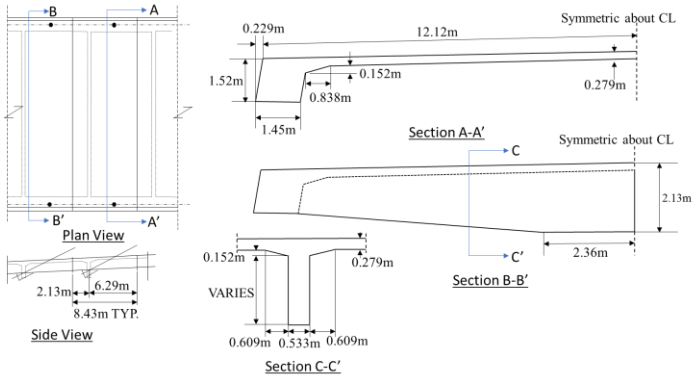

(a) Bridge Deck Plan View and Sections

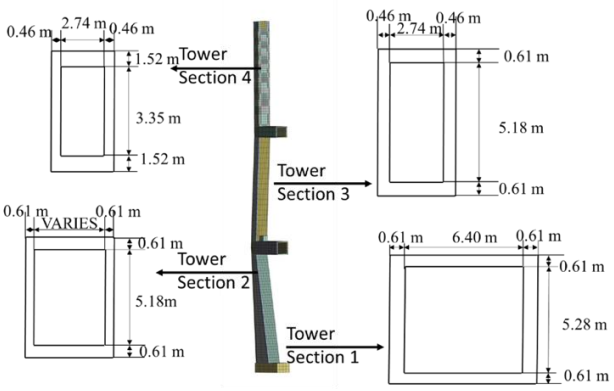

(b) Pylon Sections

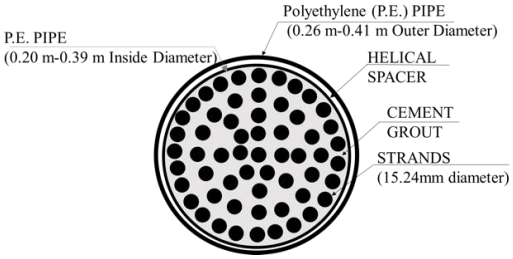

(c) Cable Cross Sections

Figure 26 - Typical Details and Sections: (a) Bridge Deck; (b) Pylon Sections; (c) Cable Cross Section.

These critical components and sections were evaluated for the three major wind load patterns. In the case of lift loading, it was necessary to evaluate the capacity of the section due to vertical bending about the transverse-axis section of the bridge deck, as shown in Fig. 25(a). For the drag case, the deck saw bending about the longitudinal-axis seen in Fig. 25(b) as well as the associated shear. For the pitch case, the deck section was checked for a combination of both lift and drag cases, as well as for torsional shear strength.

4.1.6 Analysis Results

The overall demand placed on the structure in terms of the five different hurricane categories was determined. Furthermore, the overall capacity of the critically identified sections of the Sidney Lanier bridge deck was analyzed to determine a demand-capacity ratio shown in Fig. 27. This ratio enables an analysis of these critical components at a glance and assesses how susceptible they are under the different loading scenarios. Failure, within this ratio, is defined as when the ratio is greater than or equal to one. If this is demonstrated, it is considered that yielding of the reinforcing steel in each structural section has occurred.

The demand-to-capacity ratios are presented in a bar chart. This provides a review of the analysis outcomes and a measurement of the wind loads within in each case of lift, drag, or pitch including the dynamic effects. Furthermore, this bar chart illustrates which cases of loading are significant in each hurricane category for each identified structural component in this study.

4.1.7 Critical Deck Components

Fig. 27(a) illustrates that the three wind load cases provide significant force contribution to the demand-capacity ratio in hurricane Categories between 3 and 5. Furthermore, it is identified the deck slab component as the structural component most susceptible to failure. The lateral wind

loading perpendicular to the plane of cables (or the traffic direction) is the controlling load case as illustrated by the green solid bars in Fig. 27(a). This is reasonable because the wind pressure on the cables in conjunction with the lateral loads on the bridge deck yields the most prevailing wind case and thus is potentially detrimental to the bridge deck failure as demonstrated by the demand-to-capacity ratio of 1.75 for the threshold wind speed of Category 5 hurricanes.

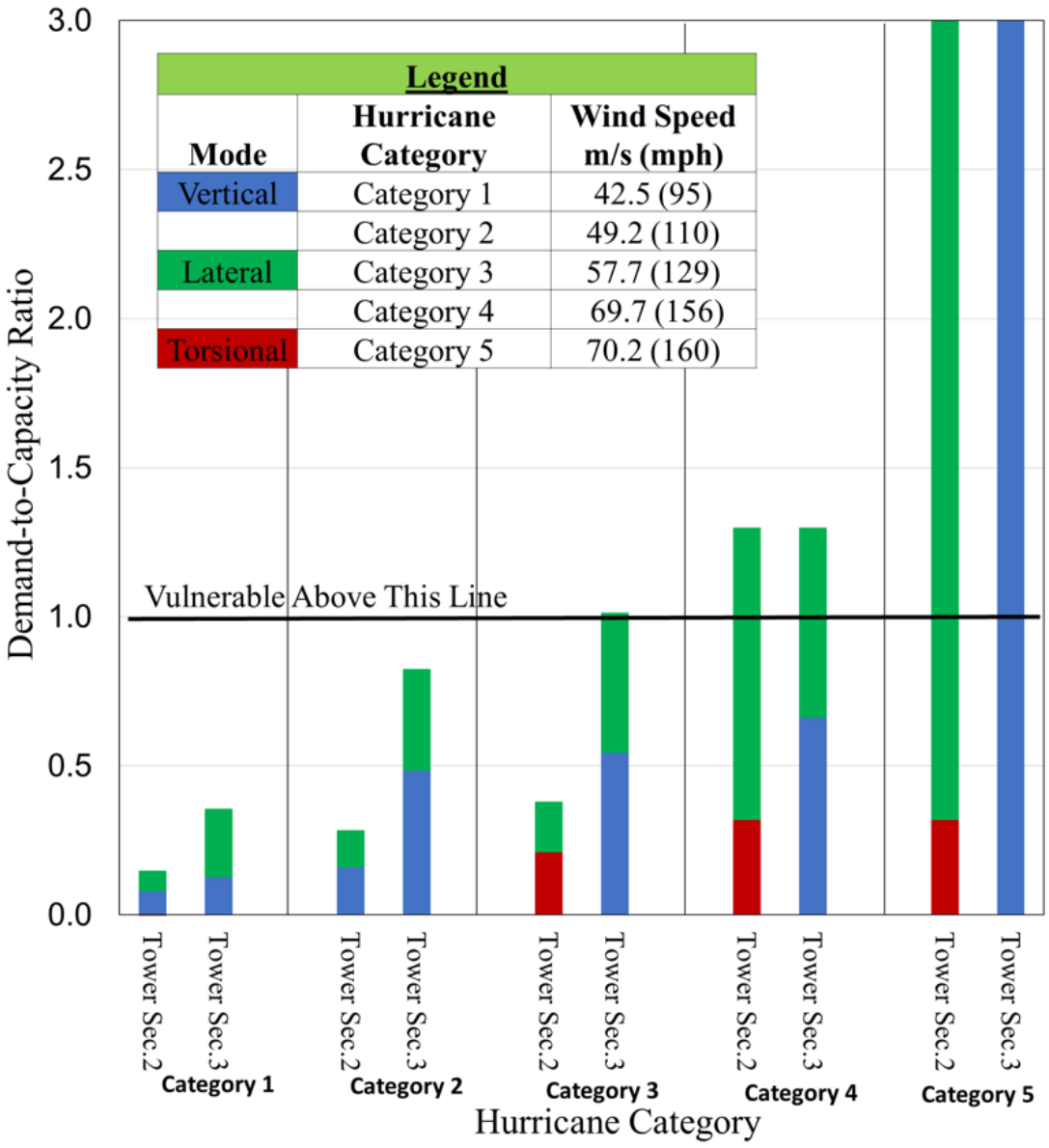

(a) Critical Tower Sections

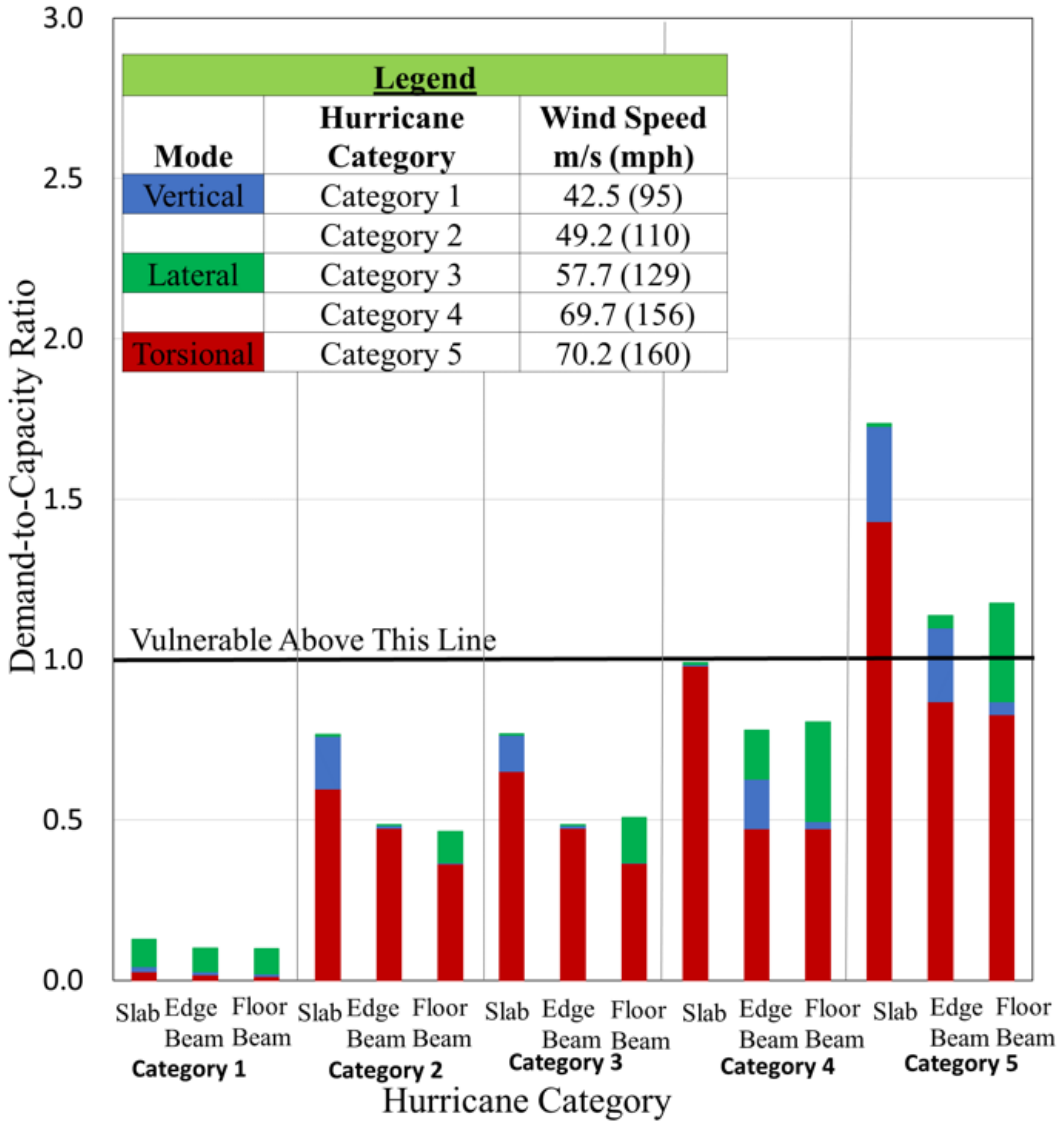

(b) Bridge Deck Components.

Figure 27 - Demand-to-Capacity Ratio: (a) Critical Tower Sections and (b) Deck Components.

4.1.8 Critical Tower Sections

The tower sections yield relatively greater demand-capacity ratios and are expected to fail in the cases of a Category 3 to 5 hurricanes. The section at the mid-height appears to be the most vulnerable for the threshold wind speed of Category 3 hurricanes. This is attributed to the lateral

wind load case including the pressure on the cables/towers and dynamic effects. The section is highly vulnerable to Category 5 hurricanes due to the torsional case reaching the demand-to-capacity ratio of 7.0 based on the linear elastic analysis. This is not illustrated within in Fig. 27(b) because the demand-to-capacity ratio is limited to 3.0.

4.1.9 Assessment of Bearing Supports and Connections

The "bar tendons" (GDOT 1996) that are used to join the elastomeric bearing pad to the deck and tower do not see large enough forces to cause failure in any of the hurricane categories.

4.2 Eugene Talmadge Memorial Bridge Analysis and Results

The same evaluation methodology which was performed for the Sidney Lanier Bridge was utilized for the Eugene Talmadge Bridge. The analysis results are discussed below. The overall demand placed on this structure in terms of the five different hurricane categories was determined. Furthermore, the overall capacity of all the critically identified sections of the Eugene Talmadge Bridge deck was analyzed to determine the demand-capacity ratio as shown in Fig. 28. This ratio enables an analysis of these critical components at a glance and assesses how susceptible they are under the different loading scenarios. Failure, within this ratio is defined as when the ratio is greater than or equal to one. If this is demonstrated, it is considered that yielding of the reinforcing steel in each structural section has occurred. This definition of failure is a non-catastrophic scenario and investigation of the redistribution of stresses after this yielding was not considered inside of this study. Even with this non-catastrophic failure criteria, collapse of the cable-stayed bridge structure could occur.

The demand-to-capacity ratios are presented in a bar chart. This chart enables a review of the analysis outcomes and contribution of the wind loads within in each case of lift, drag, or pitch including the dynamic effects. Furthermore, this bar chart illustrates which cases of loading are significant in each hurricane category for each identified structural component in this study.

4.2.1 Critical Deck Components

Fig. 28(a) illustrates that the three wind load cases provide significant force contributions to the demand-capacity ratio in hurricane Categories between 3 and 5 for the specified sections within the deck. The structural component identified as the most susceptible to failure is the deck edge beam component. The vertical wind loading due to the lift forces being exerted on the bridge is the controlling load case as illustrated by the blue solid bars in Fig. 28(a). This is due to a large lift component found within the wind tunnel investigations done for this bridge. This is potentially detrimental to the bridge deck failure as demonstrated by the demand-to-capacity ratio of 2.50 for the threshold wind speed of Category 5 hurricanes. The edge beam demand-to-capacity ratio in a Category 3 hurricane reaches a ratio of 1.16 at a wind speed of 57.7 m/s thus giving the bridge deck roughly 8.5 m/s worth of increased wind speed above the original design parameters. It is of note that the edge beam of the deck is the initial failure site rather than the deck slab. This could be due to the vertical (lift) case being the controlling load case for this deck failure. In review of the structural system of deck, the edge beams should be the first components to experience the bending rather than the slab. Since the deck can viewed as a channel beam oriented with the strong axis for the predicted lateral (drag) the loading case would be the controlling case. Thus, the weak axis is what the vertical (lift) case force has to overcome to fail the section. In this case the edge beams are the weak link in the structural system and will fail due to bending before the force will translate into the slab.

4.2.2 Critical Tower Sections

The tower sections yield relatively greater demand-capacity ratios and are expected to fail in the cases of a Category 3 - 5 hurricanes. The section at the mid-height appears to be the most vulnerable for the threshold wind speed of Category 4 hurricanes. This is attributed to the lateral wind load case including the pressure on the cables/towers and dynamic effects. The section exhibits a demand-to-capacity ratio of 1.45 within a Category 5 hurricane based on the linear elastic analysis illustrated by Fig. 28(b). The towers structural shape which exposes a large flat surface area to oncoming wind is possibly a reason for the lateral case being the controlling case for failure as seen in Fig. 28(b).

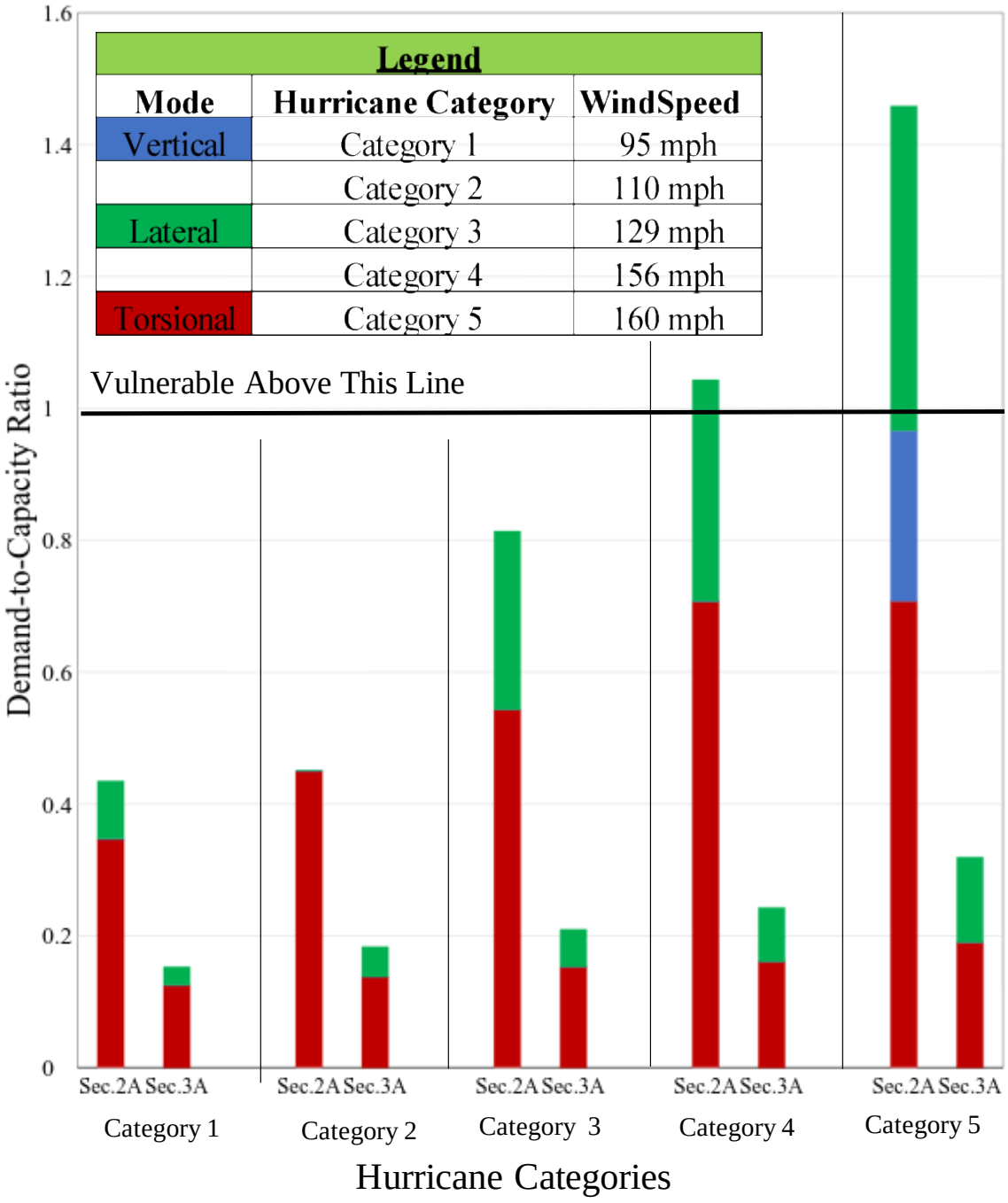

(a) Critical Tower Sections

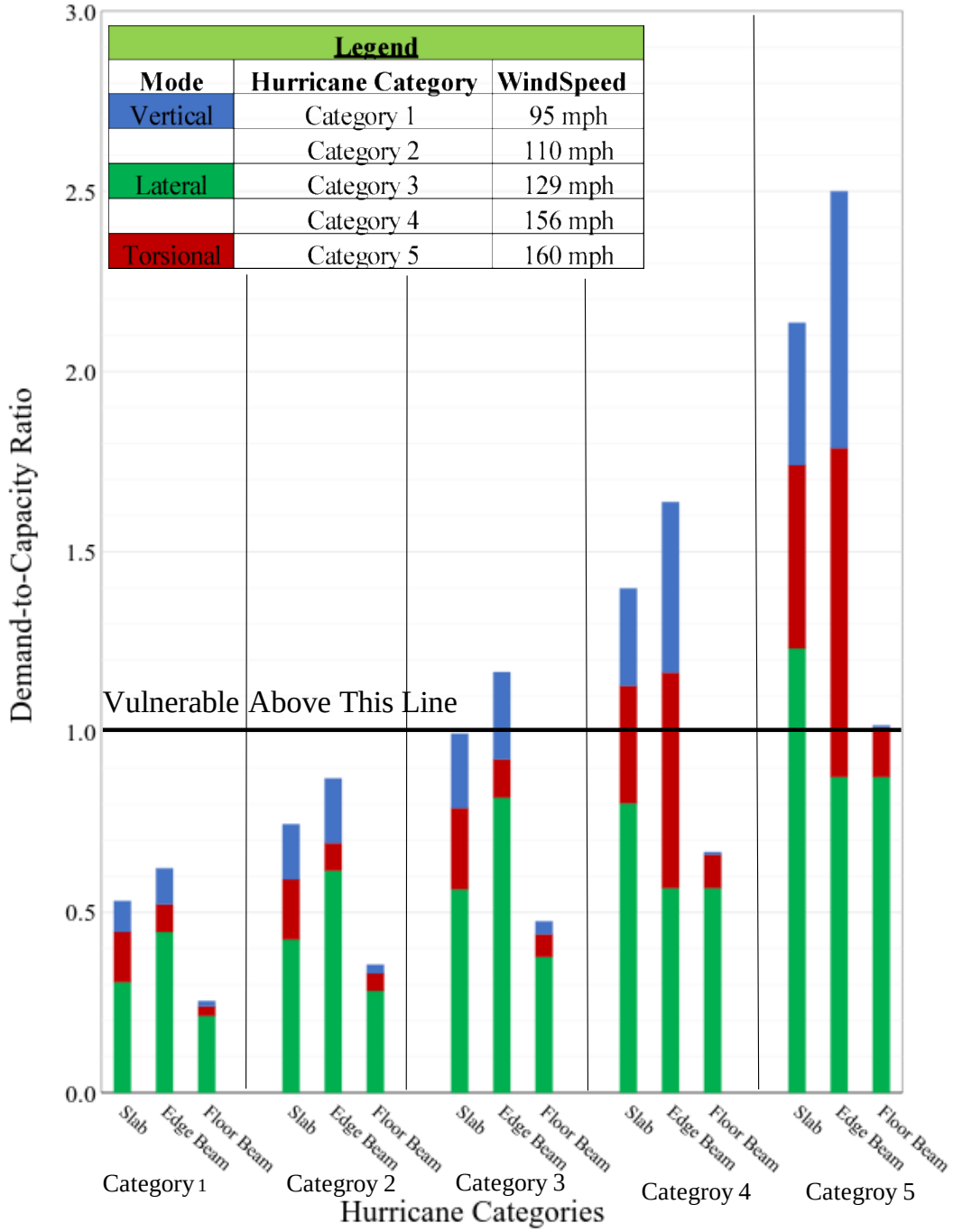

(b) Bridge Deck Components.

Figure 28 - Demand-to-Capacity Ratio: (a) Critical Tower Sections and (b) Deck Components.

While the overall geometry of both bridges under investigation is of similar nature, due to their difference in span lengths, deck widths, and tower heights, significant differences in performance was observed by this study's analysis. This is of significance since the study of cable-stayed bridges is a growing field. Therefore, designs, methodologies for analysis, and lessons learned may be shared and compared between bridges of similar and different geometry. However, it should be recognized that a direct comparison between two bridges of very similar nature cannot truly be made because the difference in geometry can lead to different static and dynamic responses that will need to be assessed on a case-by-case basis.

4.3 Comparison of Results

4.3.1 Tower Sections

The overall tower geometry for both cable-stayed bridges is very similar although there is a difference in overall tower height of 19.2 m (62ft). This difference can be attributed to the longer span of the Sidney Lanier cable-stayed bridge. As for their overall capacity, the Eugene Talmadge bridge demonstrates an ability to withstand greater hurricane wind forces as the ratio does not exceed one until the threshold wind speed of a Category 4 hurricane is considered. While the Sidney Lanier tower's demand-to-capacity ratio exceeds one in a Category 3 storm. This difference in demand-to-capacity ratios could be due to a number of different reasons. The additional height of the Sidney Lanier bridge provides a larger amount of surface area for the wind forces to strike and thus yields larger overall forces on the section. Furthermore, in reviewing both construction documents, it was found that the design of the Eugene Talmadge cable-stayed bridge implemented a more conservative reinforcing scheme for the towers. In contrast, in the Sidney Lanier Bridge having learned from the experience of the Eugene Talmadge Bridge, reduced the overall

reinforcing schedule which provided for more optimized sections for the given design criteria. While this decrease in overall reinforcing steel had an impact in the overall cost and construction of the bridge, the reduction is also seen when evaluating the bridge towers performance to beyond-design wind loading. It is concluded that the older more conservative Eugene Talmadge Bridge is be able to withstand greater beyond-basis wind forces than that of the Sidney Lanier Bridge.

4.3.2 Typical Deck Sections

Both bridges use the same basic deck geometry and are composed of a deck slab, deck edge beam, and floor beams. But there are differences in overall geometry as well. The Sidney Lanier Bridge exhibits a larger overall deck width as well as depth of the edge beams compared to that of the Eugene Talmadge Bridge. This change in geometry, while seemingly small, can have a large impact on the derived aerodynamic coefficients that the deck exhibits for drag, lift, and pitching forces. The difference in demand-to-capacity ratios is observed when reviewing their perspective bar charts above. Under close investigation, the Sidney Lanier Bridge deck does not exceed a demand-to-capacity ratio of one or greater until Category 4 hurricane wind speeds are felt, whereas the Eugene Talmadge exceeds demand-to-capacity ratio of one during Category 3 and greater hurricanes. The latter bridge has a more substantial reinforcement schedule of both mild reinforcement and post tensioned reinforcement. Despite the shorter span length and tower height and in conjunction with its increased section size and reinforcement ratio the Eugene Talmadge Bridge deck is more vulnerable to beyond-design wind loads. Furthermore, the aerodynamic coefficients determined by RWDI for each bridge show significant differences in the lateral and vertical cases as seen in Table 8 below.

Table 8 - Wind Speed and Hurricane Categories.

Aerodynamic Coeff.	Sidney Lanier	Eugene Talmadge	Percent Diff. (%)
Cx	1.4094	0.091	175.74
Cz	0.0086	0.24	186.16
Cm	0.0008	0.0016	66.67
CxTower	1.7	1.7	0.00

Seeing these large differences between the three major aerodynamic coefficients for the bridge deck, it is illustrated how the Eugene Talmadge deck sections DC ratios are greater than 1.0 at lower wind speeds whereas Sidney Lanier deck section is not.

4.4 Conclusions

While the overall geometry of both bridges under investigation is of a similar nature significant differences in performance were observed due to their differences in span lengths, deck widths, and tower heights. Designs, methodologies for analysis, and lessons learned may be shared and compared between bridges of similar and different geometry. However, it should be recognized that direct comparisons between two bridges of a very similar nature cannot truly be made. Minor differences in geometry can lead to different static and dynamic responses which must be assessed on a case-by-case basis.

5. DISCUSSION AND FUTURE WORK

Having completed evaluations of both the Sidney Lanier and Eugene Talmadge cable-stayed bridges, the critical sections identified in hurricane categories one and two do not exceed the ratio of one for both the Sidney Lanier and Eugene Talmadge Memorial cable-stayed bridges. This demonstrates that analysis procedure matches the threshold wind speeds in original design and confirms that thee obtained results can be used for a beyond design evaluation.

None of the critically identified deck sections in the Sidney Lanier bridge exceed a ratio of one during a category three hurricane. Showing that the deck itself is able to withstand wind speeds greater than the design basis. The deck slab does exceed a ratio of one in a category four hurricane, with the controlling loading scenario being lateral. All three identified components within the deck do exceed one in the case of a category five hurricane. Tower section 3 (mid tower) is vulnerable during a category three hurricane. While both tower section two and three exceed one in the case of category four and five hurricanes. The vulnerability index does reach a ratio of seven for the towers during a category five hurricane due to this study being a linear analysis, but in reality once the reinforcing steel within the section has yielded (ratio of one) there would be a redistribution of forces within the section and this ratio would not be seen. A non-linear analysis is needed to see the behavior of the bridge once the vulnerability index ratio exceeds one.

The Eugene Talmadge Memorial tower sections do not exceed a ratio of one during category three hurricanes, but the deck edge beam does reach a ratio of greater than one during a category three hurricane. With the vertical case be the controlling loading scenario for the deck edge beam. Meaning that a flexural failure about the transverse axis of the bridge deck is occurring within the edge beam. Furthermore, the deck slab is also near a ratio of one during category three hurricane and does exceed one for categories four and five. This failure of the slab would also be due to flexure about the transverse axis of the bridge deck. Interestingly, the torsional loading scenario does cause the deck edge beam and deck slab to exceed a ratio of one within a category four hurricane. Tower section two only exceeds a ratio of one for category four and five hurricanes, with the lateral loading case being the cause.

This study assumed that the wind will be at an angle of attack of zero degrees with the bridge such that it is able to have contact with the largest possible surface area. In actuality, the wind will touch the bridge at multiple different directions within a single storm; this is a loading scenario not address by this study. This study assumed linear behavior of all materials and structural properties as seen by the approach of how the wind forces are applied and the overall outcome of the results. Boundary conditions are assumed as fixed base for the towers. These were selected because they were the best choices to represent the actual conditions, although the behavior of the pile foundation base in the real world is likely to be different. The best engineering judgment is used in making these choices. The study of fluid dynamics with concerned wind is a complex topic itself.

This study assumed an air temperature of 21 degrees Celsius (70 degrees Fahrenheit) with pressure of 101 kPa (14.7 psi). Thus, the air has a density of 1.2 kg/m^3 (7.488 e-2 $\frac{lb}{ft^3}$). If air pressure or temperature changes so will the density. This will have an overall impact of the forces on the bridge. Therefore, it must be understood that this study has used very specific parameters and definitions to obtain the results shown. While the results may be used within different scenarios, it should be recognized that the results presented herein are produced to assess the vulnerability, not the progressive failure mechanism and ultimate failure analysis. These results of this study must be considered carefully within the context of the study objectives.

The future work can include the study of fatigue failure within long span bridges. Within this study the risk involving the probability of hurricane occurrence should be assessed. Further, study of the failure mechanism and collapse pattern possible for long span bridges needs to be looked into. As well as the progressive nature of failure within these structures. Finally, the instrumentation and monitoring of these studied bridges as well as other long-span bridges would be recommended so as to better asses and understand a bridges in-situ characteristics and behavior.

6. CONCLUSIONS AND RECOMANDTIONS

The results of this study demonstrate that both the Eugene Talmadge and Sydney Lanier cable-stayed bridges have capacity to withstand pressures beyond their original-designed wind speed. Their designed wind speed enabled the bridges to handle a Category 2 hurricane. This study shows that possible damage can occur in Category 3, and is more likely to occur within Categories 4 and 5. These bridges were originally constructed to replace the existing draw-bridges in both locations. The reason for the cable-stayed bridges being the choice of replacement was two-fold. First, was to reduce congestion for both the ports of Savannah and Brunswick. The previous bridges needed to be opened when ships wanted to enter since the bridges are located in each port. This was a major driving decision for choosing the cable-stayed design; cable-stay bridges allow for larger clearances between the underside of the bridge deck and the water. Secondly, this design was chosen to reduce ships' impacts into the bridge. Initial bridges were steel trusses and simple support bridges connected through a series of piers. These bridges were struck by ships on multiple occasions. The ports bring in approximately $33.2 billion in state GDP. Creating more efficient and friendly ports to large shipping vessels has been and will continue to be vital important to the state's overall economy.

An additional consequence of choosing cable-stayed bridges is that they have become focal points within their communities and have are now major tourist attractions. For example; the Talmadge Bridge has helped develop Savannah as a recreation and vacation city which continually draws a large number of visitors. Thus, if either of these two bridges were to sustain irreparable

damage or collapse, it would have the potential to have significant impact on the State economy and the Savannah and Brunswick communities. By having performed this study, the behavior of these bridges is better understood, as well as their potential for damage or vulnerability.

After reviewing the vulnerability index of the Sidney Lanier and Eugene Talmadge Memorial cable-stayed bridges the following conclusions are made:

The equivalent static wind load application procedure appropriately demonstrates dynamic mode shapes and bridge motion, this method is effective for reflecting the dynamic effects of high winds, and is practical for implementation for both cable-stayed bridges and long-span bridges. Both bridges have little reserve capacity for beyond design basis wind loads. The Sidney Lanier bridge vulnerable elements are the towers. While the Eugene Talmadge Memorial bridge vulnerable element is the deck. The dynamic wind effects were found to be significant with a ratio of static to dynamic of 1:1.3.

Using the vulnerability assessment the following comparisons between the two bridges can be made:

- A bar chart representing demand-to-capacity ratios (see Fig. 27 and 28) for the three controlling wind load cases (drag, lift, and pitch) is an effective mechanism for visualizing the most susceptible elements and illustrating the vulnerability of cable-stayed bridges in terms of hurricane categories.
- The Sidney Lanier deck section is able to withstand greater wind speeds than that of the Eugene Talmadge Memorial.

- The deck edge beam in the Eugene Talmadge Memorial bridge is the most vulnerable element, with the vertical case being the controlling loading situation .
- The deck slab is the most vulnerable element within the Sidney Lanier bridge, with the controlling loading scenario being the lateral case.
- The Sidney Lanier towers are vulnerable at a lower wind speed than the Eugene Talmadge Memorial bridge, with the lateral loading being the controlling loading scenario.
- Tower section two for the Eugene Talmadge bridge is the vulnerable section.
- Tower section three for the Sidney Lanier is the vulnerable section and is close to reaching a ratio of one for category three hurricanes.
- The analysis results reveal that the cable-stayed bridges has little reserve capacity beyond the design basis. It is strongly recommended that the bridge be closed to the public in event of major hurricanes. Although the bridge is able to withstand wind speeds beyond the design basis of 49 m/s (110 mph), there is potential for repair and/or replacement required within the range of Category 3 hurricanes, reaching the wind speed between 49 m/s (110 mph) and 57 m/s (129 mph).

At present, the Georgia Department of Transportation (GDOT) procedure is to close these bridges if any large storms or wind loads are likely to be seen on the bridges. It is recommended, based on the analysis presented in this study that this should continue. Vehicles driving over the bridge during these wind events expose a large amount of service area to the wind and it has a potential to move/damage the passengers and vehicles. If GDOT closes either bridge, procedure dictates that the bridge cannot be reopen until it passes a maintenance inspection. It is strongly recommended that this maintenance practice continue. Additional attention should be paid when wind speeds exceed the threshold of 49 m/s (110 miles per hour) for a sustained period of time

during a severe storm event. During inspection events GDOT should pay close attention the critically identified sections within studies to see if there if any large cracks have formed. Furthermore, the use of non-destructive testing and monitoring is suggested during their inspection procedure. If GDOT desires to further increase their knowledge and understanding of the bridges' behavior, it is strongly recommended they actively monitor the responses by instrumenting the bridges, monitoring their movements, and collecting different types of meaningful engineering data such as strain and acceleration measurements.

7. REFERENCES

318, ACI Committee. 2014. '318-14: Building Code Requirements for Structural Concrete and Commentary': 520.

Chorpa, Anil K. 2012. *Dynamics of Structures Theory and Applications to Earthquake Engineering* (Pearson Education).

Acampora, A., and C.T. Georgakis. 2013. 'Aerodynamic coefficients of plain and helically filleted twin circular cylinders for varying wind angles-of-attack', *International Association for Wind Engineering*.

Ahmed El-Remaily, Maher K. Tadros, Takshi Yamane, Gary Krause. 1996. 'Transverse Design of Adjacent Precast Prestressed Concrete Box Girder Bridges', *PCI*: 96-113.

Ataei, Navid 2013. 'Vulnerability Assessment of Coastal Bridges Subjected to Hurricane Events', Rice University.

Atmaca, Barbaros, Muhammet Yurdakul, and Sevket Ates. 2014. 'Nonlinear dynamic analysis of base isolated cable-stayed bridge under earthquake excitations', *Soil Dynamics and Earthquake Engineering [1984]*, 66: 314-18.

Burlina, Celeste, Christos T. Georgakis, S.V. Larsen, and Phillipp Egger. 2015. 'Preliminary Evaluation of Two New Cable Surface Innovations', *Proceedings of the 14th International Conference on Wind Engineering*.

Caetano, Elsa de Sa. 2007. 'Cable Vibrations in Cable-Stayed Bridges', *Association for Bridge and Structural Engineering (IBS)-Association Internationale des Ponts et Charpentes (AIPC)-Internationale Vereinigung fur Bruckenbau und Hochbau (IVBH*.

Camara, A., K. Nguyen, A. M. Ruiz-Teran, and P. J. Stafford. 2014. 'Serviceability limit state of vibrations in under-deck cable-stayed bridges accounting for vehicle-structure interaction', *Engineering Structures*, 61: 61-72.

Chen, Xinzhong. 2015. 'Analysis of Multimode Coupled Buffeting Response of Long-Span Bridges to Nonstationary Winds with Force Parameters from Stationary Wind. ', *Journal of Structural Engineering*, 141.

Chen, Xinzhing, and Ahsan Kareem. 2001. 'Equivalent Static Wind Loads for Buffeting Response of Bridges', *Journal of Structural Engineering*: 1467-75.

Cheng, S. H., and David T. Lau. 2002. 'Modeling of cable vibration effects of cable-stayed bridges', *Earthquake Engineering and Engineering Vibration*, 1: 74-85.

Corven, John. 2015. 'Post-Tensioned Box Girder Design Manual', *U.S. Department of Transportation Federal Highway Administration*.

Das, R., A. D. Pandey, Soumya, M. J. Mahesh, P. Saini, and S. Anvesh. 2016. 'Progressive Collapse of a Cable Stayed Bridge', *Procedia Engineering*, 144: 132-39.

Davenport, A.G. 1964. 'Note On the Distribution of the Largest Value of a Function with Application to Gust Loading', *Proceedings - Institution of Civil Engineers*, 28: 187-96.

Davenport, A.G. 1967. 'Gust Loading Factors', *ASCE - Journal of the Structural Division*: 11-34.

Davenport, A.G. 1985. 'The Representation of the Dynamic Effects of Turbulent Wind by Equivalent Static Loads', *The Proceedings: The 1985 International Engineering Symposium on Structural Steel*: 1-13.

Davenport, A.G., and J.P.C King. 1984. 'Dynamic Wind Forces on Long Span Bridges': 705-12.

El Ouni, M. H., N. Ben Kahla, and A. Preumont. 2012. 'Numerical and experimental dynamic analysis and control of a cable stayed bridge under parametric excitation', *Engineering Structures*, 45: 244-56.

Fu, Jiyang, Zhuanging Xie, and Q.S. Li. 2008. 'Equivalent Static Wind Loads on Long-Span Roof Structures', *ASCE - Journal of Structural Engineering*: 1115-11128.

Georgia Department of Transportation (1996). GeoPI http://www.dot.ga.gov/BS/Projects/ProjectSearch Accessed May 31 2016.

Han, Houzeng, Jian Wang, Xiaolin Meng, and Hua Liu. 2016. 'Analysis of the dynamic response of a long span bridge using GPS/accelerometer/anemometer under typhoon loading', *Engineering Structures*, 122: 238-50.

Holmes, J.D. 2002. 'Effective Static Load Distributions in Wind Engineering', *Journal of Wind Engineering & Industrial Aerodynamics*, 90: 91-109.

Huynh, Thanh-Canh, Jae-Hyung Park, and Jeong-Tae Kim. 2016. 'Structural identification of cable-stayed bridge under back-to-back typhoons by wireless vibration monitoring', *Measurement*, 88: 385-401.

Iriwin, Peter A., Jiming Xie, Stoyan T. Stoyanoff, and Gordon E. Dunn. 1995. 'Experiences in Wind Tunnel Testing of Long Span Bridges', *International Bridge Conference 12th Annual International Bridge Conference and Exhibition*: 63-69.

Jones, N., and E. Ozkan. 2002. "Wind Effects on Long Span Cable Stayed Bridges: Assessment and Validation." In, edited by S. A. Cauffman, 121-32. National Institute of Standards and Technology.

Jones, N. P., R. H. Scanlan, A. Jain, and H. Katsuchi. 1998. "Advances (and challenges) in the prediction of long-span bridge response to wind." In, edited by A. Larsen and S. Esdahl, 59-86. A A Balkema Publishers.

Kawatani, M., H. Kim, H. Uejima, and H. Kobayashi. 1993. 'EFFECTS OF TURBULENT FLOWS ON VORTEX-INDUCED OSCILLATION OF BRIDGE GIRDERS WITH BASIC SECTIONS', *JOURNAL OF WIND ENGINEERING AND INDUSTRIAL AERODYNAMICS*, 49: 477-86.

Keerthana, M., and P. Harikrishna. 2013. 'Application of CFD for assessment of galloping stability of rectangular and H-sections', *JOURNAL OF SCIENTIFIC & INDUSTRIAL RESEARCH*, 72: 419-27.

Kim, Byeong-Cheol, and Sung-Soon Yhim. 2014. 'Buffeting Analysis of a Cable-Stayed Bridge Using Three-Dimensional Computational Fluid Dynamics', *Journal of Bridge Engineering*, 19: -1.

King, J. Peter. 1999. 'Integrating Wind Tunnel Test of Full Aerolastic Models into the Design of Long Span Bridges', *Wind Engineering into the 21st Century: Proceedings of the Tenth Conference on Wind Engineering*, 2: 927-34.

Kleissl, K., and C.T. Georgkis. 2012. 'Comparison of the Aerodynamic of Bridge Cables with Helical Fillets and a Pattern-Indented Surface', *Journal of Wind Engineering & Industrial Aerodynamics*: 166-75.

Larsen, Allan, and Guy L. Larose. 2015. 'Dynamic wind effects on suspension and cable-stayed bridges', *Journal of Sound and Vibration*, 334: 2-28.

Lepidi, Marco, and Vincenzo Gattulli. 2016. 'Non-linear interactions in the flexible multi-body dynamics of cable-supported bridge cross-sections', *International Journal of Non-Linear Mechanics*, 80: 14-28.

Li, Hui, Wen-Li Chen, Feng Xu, Feng-Chen Li, and Jin-Ping Ou. 2010. 'A numerical and experimental hybrid approach for the investigation of aerodynamic forces on stay cables suffering from rain-wind induced vibration', *Journal of Fluids and Structures*, 26: 1195-215.

Li, Shouying, Zhengqing Chen, Teng Wu, and Ahsan Kareem. 2013. 'Rain-Wind-Induced In-Plane and Out-of-Plane Vibrations of Stay Cables', *Journal of Engineering Mechanics*, 139: 1688-98.

Loh, C. H., and C. M. Chang. 2007. 'MATLAB-based seismic response control of a cable-stayed bridge: cable vibration', *STRUCTURAL CONTROL & HEALTH MONITORING*, 14: 109-43.

Lonetti, P., and A. Pascuzzo. 2014. 'Vulnerability and failure analysis of hybrid cable-stayed suspension bridges subjected to damage mechanisms', *Engineering Failure Analysis*, 45: 470-95.

Lozano-Galant, Jose Antonio, Maria Nogal, Ignacio Paya-Zaforteza, and Jose Turmo. 2014. 'Structural system identification of cable-stayed bridges with observability techniques', *Structure & Infrastructure Engineering: Maintenance, Management, Life-Cycle Design & Performance*, 10: 1331-44.

Mannini, C., and G. Bartoli. 2015. 'Aerodynamic uncertainty propagation in bridge flutter analysis', *Structural Safety*, 52: 29-39.

Mansell, Erin J., Paul D. Docherty, J. Geoffery Chase, and Balázs Benyó. 2015. 'An eigen-analysis of the relationships between model structure, discrete data, measurement error and resulting parameter identification distributions', *IFAC PapersOnLine*, 48: 88-93.

Officials, American Association of State Highway and Transportation. 2012. 'AASHTO LRFD Bridge Design Specifications'.

P.Jones, Nicholas, Robert H. Scanlan, Anurag Jain, and Hirishi Katsuchi. 1998. 'Advances (and challenges) in the prediction of long-span bridge response to wind', *Bridge aerodynamics*: 59-95.

Padgett, J. E., Nielson, B. G., & DesRoches, R. . 2008. 'Selection of optimal intensity measures in probabilistic seismic demand models of highway bridge portfolios', *EARTHQUAKE ENGINEERING & STRUCTURAL DYNAMICS*, 37: 711-25.

Pakos, Wojcieh, and Zbigniew Wójcicki. 2014. 'Vibration Control f a Cable-Stayed Footbridge Using the Tension Changes of Cable', *XXIII R-S-P Seminar, Theoretical Foundation of Civil Engineering(23RSP) (TFoCE 2014)*.

Raftoyiannis, Ioannis G., and George T. Michaltsos. 2012. 'CURVED-IN-PLANE CABLE-STAYED BRIDGES:: A MATHEMATICAL MODEL', *International Journal of Structural Stability & Dynamics*, 12: 1250011-1-11-41.

Raftoyiannis, Ioannis G., and George T. Michaltsos. 2015. 'A Mathematical Model For Cables Provided With Dampers', *International Journal of Bridge Engineering*, 3: 11-32.

Raggett, Jon D. 2016. 'Long-Span Cable-Supported Bridges' Performance Improvements in Extreme Winds: Five Case Studies', 26: 6.

Rowan Williams Davies & Irwin (RWDI), Inc. (1997). “Wind Engineering Studies For Sidney Lanier Bridge Glynn County Georgia”, Project No. 94-198.

Savaliya, Ghanshyam M., Atul K. Desai, and Sandeep A. Vasanwala. 2013. 'Effects of the Cable-Stays Configuration on the Behavior of Long Span Cable-Stayed Bridge', *IUP Journal of Structural Engineering*, 6: 7-16.

Schemmann, Armin G., and H. Allison Smith. 1998. 'Vibration Control of Cable-Stayed Bridges Part 1: Modeling Issues', *Earthquake Engineering & Structural Dynamics*, 27: 335.

Schemmann, A. G., and H. A. Smith. 1998. 'Vibration control of cable-stayed bridges - Part 2: Control analyses', *EARTHQUAKE ENGINEERING & STRUCTURAL DYNAMICS*, 27: 825-43.

Starossek, Uwe. 1998. 'Bridge Instability in Wind and Spatial Flutter Analysis', *KOREAN SOCIETY OF CIVIL ENGINEERS*, 1: 9-20.

Studničková, Marie. 1986. 'Investigation of wind effects on a multi-cable-stayed bridge with prestressed concrete', *Journal of Wind Engineering & Industrial Aerodynamics*, 23: 465-76.

Sukamta, Ireng Guntorojati, and Fariduzzaman. 2017. 'Flutter analysis of cable stayed bridge', *Procedia Engineering*, 171: 1173-77.

Sun, Bo, Paolo Gardoni, and Rucheng Xiao. 2016. 'Probabilistic aerostability capacity models and fragility estimates for cable-stayed bridge decks based on wind tunnel test data', *Engineering Structures*, 126: 106-20.

Trivedi, Hardik. 2014. 'Segmental Bridge Design of Prestressed Box Superstructure For Cantilever Construction', *International Journal of Bridge Engineering*, 2: 49-82.

Weight, A. J. 2009. 'Critical Analysis of the Great Belt East Bridge, Denmark', *Proceedings of Bridge Engineering*.

Wu, Teng, and Ahsan Kareem. 2012. 'An Overview Of Vortex-Induced Vibration (VIV) Of Bridge Decks', *Frontiers of Structural & Civil Engineering*, 6: 335.

Wu, Teng, and Ahsan Kareem. 2013. 'Bridge aerodynamics and aeroelasticity: A comparison of modeling schemes', *Journal of Fluids and Structures*, 43: 347-70.

Xuewei, Wang, Zhu Bing, and Cui Shengai. 2017. 'Research on Collapse Process of Cable-Stayed Bridges under Strong Seismic Excitations', *Shock and Vibration, Vol 2017 (2017)*.

Yang, Yong-Xin, and Yao-Jun GE. 2012. 'Wind-Induced Vibrations and Equivalent Static Wind Loading for Cable-Stayed Bridges', *The Seventh International Colloquium of Bluff Body Aerodynamics and Applications*: 399-409.

Yazdani-Paraei, H., H. Moharrami, S. Maalek, and M. Heydari. 2012. 'Optimum design of cable-stayed bridges', *Australian Journal of Structural Engineering*, 12: 99-118.

Zhao, Yueyu, and Houjun Kang. 2008. 'In-plane free vibration analysis of cable–arch structure', *Journal of Sound and Vibration*, 312: 363-79.

Zuo, Delong, and Nicholas P. Jones. 2010. 'Interpretation of field observations of wind- and rain-wind-induced stay cable vibrations', *Journal of Wind Engineering & Industrial Aerodynamics*, 98: 73-87.